Acta Cryst C
STRUCTURAL CHEMISTRY

ISSN 2053-2296

Isolation and crystal and molecular structures of $[(C_5H_2Br_3)_2Fe]$, $[(C_5HBr_4)_2Fe]$ and $[(C_5Br_5)(C_5Br_4HgBr)Fe]$

Tobias Blockhaus and Karlheinz Sünkel*

Chemistry, Ludwig-Maximilians-University Munich, Butenandtstrasse 5-13, Munich, D-81377, Germany. *Correspondence e-mail: suenk@cup.uni-muenchen.de

Received 22 June 2022
Accepted 28 September 2022

Edited by T. Roseveare, University of Sheffield, United Kingdom

Keywords: noncovalent interactions; halogen bonding; Hirshfeld analysis; crystal structure; bromoferrocene.

CCDC references: 2210089; 2210088; 2210087

Supporting information: this article has supporting information at journals.iucr.org/c

The reaction of $[(C_5H_3Br_2)_2Fe]$ with lithium tetramethylpiperidinide (LiTMP) in a 1:10 molar ratio in tetrahydrofuran yields, after quenching with $C_2H_2Br_4$, a mixture of the polybromoferrocenes $[C_{10}H_{10-n}Br_nFe]$ with n = 4–9, from which single crystals of bis(1,2,3-tribromocyclopentadienyl)iron(II), $[Fe(C_5H_2Br_3)_2]$, and bis(1,2,3,4-tetrabromocyclopentadienyl)iron(II), $[Fe(C_5HBr_4)_2Fe]$, were obtained by a combination of chromatography and fractional crystallization. Treatment of '$[C_{10}(HgOAc)_{10}Fe]$' with KBr_3 yields a mixture of polybromoferrocenes $[C_{10}H_{10-n}Br_nFe]$ with n = 8–10 and bromomercurioferrocenes $[C_{10}H_{9-n}Br_n(HgBr)Fe]$ with n = 7–9, from which single crystals of (1-bromomercurio-2,3,4,5-tetrabromocyclopentadienyl)(1,2,3,4,5-pentabromocyclopentadienyl)iron(II), $[FeHgBr(C_5Br_4)(C_5Br_5)]$, were obtained by fractional crystallization. The crystal structures of all the compounds show Br$\cdots$Br, Br$\cdots$H and sometimes Br$\cdots$Cp$\cdots\pi$ (Cp is a ring centroid) interactions, as well as π–π interactions. The findings are supported by Hirshfeld analyses.

1. Introduction

'Noncovalent interactions' are found in nearly all disciplines of chemistry, biochemistry and biology, and have been studied, at least in part, for quite a while (Hobza & Řezáč, 2016). This term brings together such apparently different interactions as hydrogen, halogen, lone-pair–π, anion–π, cation–π and π–π bonding, and these interactions can either act independently or co-operatively (Mahadevi & Sastry, 2016; Portela & Fernández, 2021). Among these, halogen bond(ing) has been studied continuously at a high level since about 1995. The last comprehensive review dates back to 2016 (Cavallo *et al.*, 2016). A look at *SciFinder* shows since then nearly 2000 new entries for the years 2021 and 2022, and already 492 entries with the concept 'Halogen Bonding' (accessed on May 26th, 2022). The vast majority of these studies are centred on organic or biological systems, with a focus on crystal engineering (Mukherjee *et al.*, 2014). Relatively rarely studied were metal-containing systems (Brammer *et al.*, 2008), in particular, organometallic systems have so far been restricted to a few metal carbonyls, ruthenium-complexed aryl iodides (Kelly & Holman, 2022) and one study on 1,1′-dihaloferrocenes (Shimizu & Ferreira da Silva, 2018). Our group has been working on polyhalogenated metallocenes for quite a while (Sünkel & Motz, 1988; Sünkel & Hofmann, 1992; Sünkel *et al.*, 1994, 2015; Sünkel & Bernhartzeder, 2011), and some very recent reports on the synthesis and crystal structure determinations of $[(C_5H_nBr_{5-n})(C_5H_2Br_3)Fe]$ (n = 1 or 2; Butler *et al.*, 2021; Butler, 2021) and $[(C_5H_nBr_{5-n})(C_5Br_5)Fe]$ (n = 0 or 1; Rupf *et al.*, 2022) prompted us to report on our synthetic and

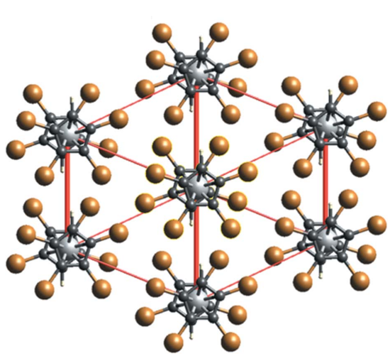

Table 1
Experimental details.

Experiments were carried out with Mo $K\alpha$ radiation.

	3	**5**	**8**
Crystal data			
Chemical formula	$[Fe(C_5H_2Br_3)_2]$	$[Fe(C_5HBr_4)_2]$	$[FeHgBr(C_5Br_4)(C_5Br_5)]$
M_r	656.69	817.25	1175.64
Crystal system, space group	Triclinic, $P\overline{1}$	Triclinic, $P\overline{1}$	Monoclinic, $P2_1/n$
Temperature (K)	153	103	295
a, b, c (Å)	7.0903 (3), 7.4318 (5), 13.8071 (5)	6.9395 (2), 7.0548 (2), 8.9271 (3)	8.9784 (3), 14.0971 (4), 15.8485 (4)
α, β, γ (°)	88.745 (4), 84.993 (3), 77.728 (4)	67.577 (1), 76.160 (1), 86.461 (1)	90, 90.689 (1), 90
V (Å^3)	708.21 (6)	392.06 (2)	2005.79 (10)
Z	2	1	4
μ (mm^{-1})	17.86	21.33	28.28
Crystal size (mm)	0.49 × 0.15 × 0.05	0.03 × 0.01 × 0.01	0.06 × 0.02 × 0.02
Data collection			
Diffractometer	Agilent XCalibur 2	Bruker D8 Venture	Bruker D8 Venture
Absorption correction	Multi-scan (*CrysAlis PRO*; Agilent, 2014)	Multi-scan (*TWINABS*; Bruker, 2012)	Multi-scan (*SADABS*; Krause *et al.*, 2015)
T_{min}, T_{max}	0.434, 1.000	0.180, 0.344	0.193, 0.332
No. of measured, independent and observed [$I > 2\sigma(I)$] reflections	9297, 3234, 2496	3772, 3772, 3107	33353, 4098, 3154
R_{int}	0.041	–	0.050
$(\sin \theta/\lambda)_{max}$ (Å^{-1})	0.649	0.832	0.625
Refinement			
$R[F^2 > 2\sigma(F^2)]$, $wR(F^2)$, S	0.043, 0.090, 1.09	0.037, 0.076, 1.06	0.036, 0.092, 1.06
No. of reflections	3234	3772	4098
No. of parameters	162	89	199
No. of restraints	2	0	0
H-atom treatment	H-atom parameters constrained	H-atom parameters constrained	–
$\Delta\rho_{max}$, $\Delta\rho_{min}$ (e Å^{-3})	2.31, −0.97	1.32, −1.31	1.63, −1.24

Computer programs: *CrysAlis PRO* (Agilent, 2014), *APEX2* (Bruker, 2012), *SAINT* (Bruker, 2011), *SHELXT2014* (Sheldrick, 2015*a*) and *SHELXL2018* (Sheldrick, 2015*b*).

crystallographic studies of polybromoferrocenes. A special focus is made on the occurrence of halogen and hydrogen bonding in these systems.

2. Experimental

2.1. Synthesis and crystallization

2.1.1. Reaction of 1,1′,2,2′-tetrabromoferrocene (1) with LiTMP in a 1:10 molar ratio and $C_2H_2Br_4$. A solution of **1** (243 mg, 0.48 mmol) in tetrahydrofuran (THF; 2 ml) was added to a freshly prepared solution of LiTMP (4.8 mmol) in THF (4 ml) at −30 °C. After stirring for 5 h, the temperature was lowered to −78 °C and $C_2H_2Br_4$ (0.6 ml, 5.0 mmol) was added. With continuous stirring, the temperature was raised to ambient temperature over a period of 16 h. After this, water (10 ml) was added and the mixture was extracted with several 10 ml portions of CH_2Cl_2. The combined extracts were washed with water, then dried with $MgSO_4$ and completely evaporated *in vacuo*. The residue was taken up in the minimum amount of petroleum ether and chromatographed on an alumina column (20 × 2 cm), using petroleum ether as eluent. 21 fractions were collected and examined by mass spectroscopy and selected fractions were examined by ^{1}H NMR spectroscopy (Figs. S1 and S2 in the supporting information). All fractions contained mixtures of polybromoferrocenes. While the first fraction consisted of a mixture of penta-, hexa- and heptabromoferrocene, the intermediate fractions contained hexa-, hepta- and octabromoferrocene, and the last fraction was a mixture of hepta- and octabromoferrocene with traces of nonabromoferrocene. Crystals of 1,1′,2,2′,3,3′-hexabromoferrocene (**3**) were obtained by slow evaporation of the sixth fraction in a refrigerator, and crystals of 1,1′,2,2′,3,3′,4,4′-octabromoferrocene (**5**) were obtained from the last fraction by the same method. All other fractions were also recrystallized from different solvents (petroleum ether, Et_2O and CH_2Cl_2), but yielded neither crystals nor 'pure' powders (according to ^{1}H NMR spectra taken after redissolution).

Hexabromoferrocene (**3**). ^{1}H NMR (270 MHz, $CDCl_3$): δ 4.47 ppm (literature: 4.47 ppm; Butler, 2021). MS (DEI): m/z = 659.6 (calculated 659.5).

Octabromoferrocene (**5**). ^{1}H NMR (400 MHz, DMSO-d_6): δ 5.20 ppm. MS (DEI): m/z = 817.4 (calculated 817.3).

2.1.2. Reaction of '$[C_{10}(HgOAc)_{10}Fe]$' with KBr_3. A suspension of 'permercurated ferrocene' (2.78 g, *ca* 1 mmol) with KBr_3, freshly prepared from KBr (1.19 g, 10 mmol) and Br_2 (0.512 ml, 10 mmol) in water (100 ml), was stirred for 4 h at room temperature. After filtration, the residue was first washed with water and then extracted with dichloromethane. The combined extracts were evaporated *in vacuo* and the residue was placed on top of an alumina column. A 1:1 mixture of petroleum ether and dichloromethane eluted two yellow bands. The first fraction consisted, according to its mass spectrum (Fig. S3), of a mixture of deca-, nona- and octabromoferrocene, while the second fraction yielded a mixture of the bromomercurioferrocenes $[C_{10}H_nBr_{9-n}HgBrFe]$ with n =

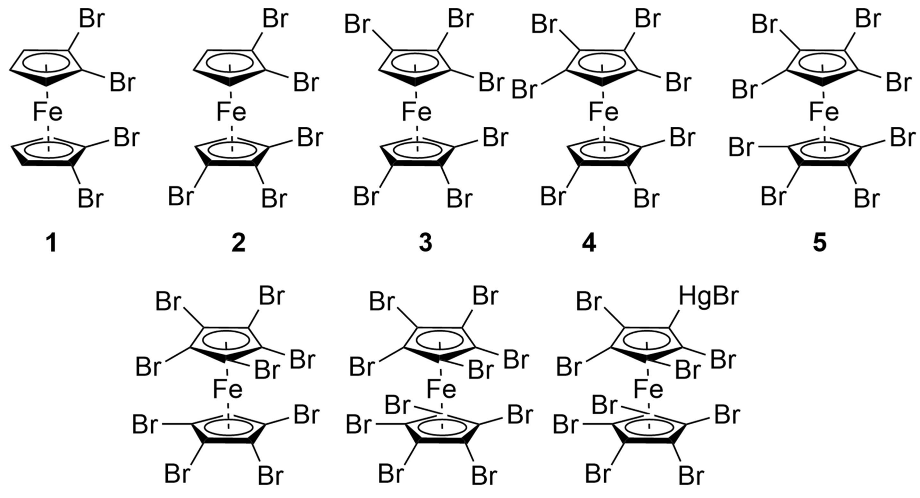

Figure 1
The structural formulae of compounds **1**–**8**.

0–2 (Fig. S4). The [1]H NMR spectrum of the first fraction showed four weak signals, which unfortunately could not be assigned to individual compounds (Fig. S5). Recrystallization attempts with the first fraction yielded again only mixtures, while from the second fraction, crystals of [$(C_5Br_5)(C_5Br_4$-HgBr)Fe] (**8**) could be obtained.

2.2. Refinement

Compound **3**: *SHELXT* (Sheldrick, 2015*a*) provided the complete molecule of **3** on the first run. The following difference Fourier synthesis (see Fig. S6 of the supporting information) showed two electron-density maxima (Q15 and Q16 in Fig. S6; d = 2.66 and 2.48 e Å^{-3}) at radial distances of 1.54 and 1.40 Å from ring atoms C24 and C14, respectively. Despite these short distances (more typical for C—C bonds), we assigned these peaks to Br atoms (first named X1 and X2) with very low site-occupancy factors, since from the preceeding synthesis no other elements could have been present. The following refinement, however, showed rather short intermolecular distances (2.581/3.328 and 2.955/3.106 Å) from these positions to atoms Br21^{i}/Br22^{i} and Br11^{i}/Br12^{i}, respectively [symmetry code: (i) x, $y - 1$, z] (Fig. S7). It was concluded that X1/X2 could not be present in the same molecule as Br11/Br12/Br21 (and eventually Br22 also) and therefore it was assumed that compound **3** (with Br11–Br13 and Br21–Br23) cocrystallized with very small amounts (*ca* 3%) of compound **2** [with Br13–Br14 (= X2) and Br22–Br24 (= X1)], and this model was used for the subsequent refinements. The refinement procedure was as follows: first, it was assumed that all Br atoms would have the same isotropic U values and then the site-occupation factors for X1 = Br24/H24 and X2 = Br14/H14, as well as Br11/H11, Br12/H12, Br21/H21 and Br23/H23, were allowed to refine. The site-occupancy factors were then fixed at these values and the U values were allowed to refine freely for the main components even anisotropically. Any attempts to produce longer C14—Br14 and C24—Br24 'bonds' *via* the use of restraints met with failure. It should be noted at this point that the crystal structure of 1,1′,2,4-tetraiodoferrocene showed a similar disorder and an apparent 'bond shortening', which the authors were able to resolve (Evans *et al.*, 2021).

Compound **5**: the measured crystal was recognized as a twin (two domains, rotated by 180° around 010) and a HKLF5 data file was created. The scale factor BASF refined to a final value of 0.17818. The refinement proceeded without any problems, and no signs of disorder were found.

Crystal data, data collection and structure refinement details of all compounds are summarized in Table 1.

3. Results and discussion

3.1. Synthesis

According to a recent review on haloferrocenes, there were only three heteroannularly substituted polybromoferrocenes known in 2018 (Butenschön, 2018): 1,1′-dibromoferrocene, 1,1′,2-tribromoferrocene and decabromoferrocene. Since then, at least one isomer of each of the remaining [$C_{10}H_n$-Br_{10-n}Fe] with n = 4–9 has been obtained, sometimes only as part of mixtures. There were two different synthetic approaches to achieve this: (i) stepwise lithiation followed by electrophilic quenching with 'Br^+', starting with 1,1′-dibromoferrocene, or (ii) 'permercuration' of ferrocene followed by treatment with KBr_3. Both methods had their shortcomings, however. When 1,1′-dibromoferrocene was treated with 2.1 equivalents of LiTMP in THF at low temperature, followed by electrophilic quenching with 1,1,2,2-tetrabromoethane, a mixture of tri-, tetra-, penta-, hexa-, hepta- and octabromoferrocenes was obtained, from which the first two could be obtained in pure form (yields of 9.9 and 16.0%, respectively; Butler *et al.*, 2021). When the solvent was changed from THF to hexane, the electrophile to dibromohexafluoropropane and the temperature to room temperature, 1,1′,2,2′-tetrabromoferrocene (**1**) was obtained in over 90% yield (Butler, 2021). Repeating the latter procedure on compound **1** gave rather

Table 2
Overview of the CSD structures of polyhaloferrocenes substituted on both rings.

Chemical formula	Abbreviation in this text	Refcode in the CSD	Conformation	Reference
$C_{10}H_8F_2Fe$	FdF_2	RACROF	Eclipsed, **I**	Inkpen *et al.* (2015)
$C_{10}H_8Cl_2Fe$	$FdCl_2$	DUTSUH, DUTSUH01	Eclipsed, **I**	Bryan & Leadbetter (1986); Inkpen *et al.* (2015)
$C_{10}H_8Br_2Fe$	$FdBr_2$	BIPDOU	Eclipsed, **I**	Hnetinka *et al.* (2004)
$C_{10}H_8I_2Fe$	FdI_2	KOPFAY	Staggered	Roemer & Nijhuis (2014)
$C_{10}H_7Br_3Fe$	$FdBr_3$	UTOBIR	Nearly eclipsed, **VI**	Butler *et al.* (2021)
$C_{10}H_7I_3Fe$	FdI_3	EZAWUA	Nearly eclipsed, **VI**	Evans *et al.* (2021)
$C_{10}H_6Cl_4Fe$	$FdCl_4$	CEVBEK	Eclipsed, **IV**	Sato *et al.* (1984)
$C_{10}H_6Br_4Fe$	$FdBr_4$	UTOBUD	Eclipsed, **IV**	Butler *et al.* (2021)
$C_{10}H_6I_4Fe$-	FdI_4	EZAWOU	Eclipsed, **VI**	Evans *et al.* (2021)
$C_{10}H_4Cl_6Fe$	$FdCl_6$	DUTSUG	No data in CSD	Bryan & Leadbetter (1986)
$C_{10}HBr_9Fe$	$FdBr_9$	FEFZAV	Staggered	Rupf *et al.* (2022)
$C_{10}Br_{10}Fe$	$FdBr_{10}$	FEFYUO	staggered	Rupf *et al.* (2022)

high yields of 1,1′,2,2′,3,3′-hexabromoferrocene (**3**), contaminated, however, with heptabromoferrocene (**4**) and octabromoferrocene (**5**). All attempts to repeat this procedure on compound **3** met with failure, due to the very low solubility of this compound. On the other hand, the preparation of 'permercurated ferrocenes' followed by the addition of KBr_3, first reported in 1977, then later in 1994, 1997 and 2022, suffered from difficulties due to solubility problems (Boev & Dombrovskii, 1977; Han *et al.*, 1994; Neto *et al.*, 1997; Rupf *et al.*, 2022). For example, Han and co-workers showed that using $Hg(O_2CCF_3)_2$ as the mercuration agent gave a 'mixture of at least four partially brominated ferrocenes'. When they used $Hg(O_2CCH_3)_2$ as the mercuration agent, decabromoferrocene (**7**) could be isolated in 60% yield, contaminated, however, with at least two partially brominated ferrocenes. Rupf and co-workers repeated this latter experiment and showed that besides **7** also nonabromoferrocene (**6**) and nonabromo(bromomercurio)ferrocene (**8**) were formed (based on ^{13}C NMR spectroscopy; a closer look at Fig. S20 of their supporting information shows the additional formation of octabromoferrocene **5** and the bromomercurioferrocenes [$C_{10}H_nBr_{9-n}HgBrFe$] with n = 1 and 2). When they used $Hg(O_2CC_3H_7)_2$, they apparently obtained a mixture of **7** and **8** with no other contaminants (based on NMR and IR). Neto and co-workers reported the use of $Hg(O_2CCCl_3)_2$ as the mercuration agent, the transformation of the apparently formed [$C_{10}(HgO_2CCl_3)_{10}Fe$] to the decachloromercurioferrocene, followed by reaction with KBr_3 to give pure **7** [characterization by NMR and IR spectroscopy, and elemental analysis (C and Fe)].

We decided to look at the lithiation reactions with LiTMP as the lithiating reagent, $C_2H_2Br_4$ as the brominating agent and THF as the reaction medium at low temperatures again. We started with a solution of 1,1′,2,2′-tetrabromoferrocene (**1**; purity > 95%) in THF and treated it with ten molar equivalents of LiTMP, followed by the addition of tetrabromoethane. After standard work-up, a chromatographic separation was attempted. Since no band formation was recognizable, 21 fractions with equal volume were collected. Fractions 1, 10, 12 and 21 were examined by mass spectrometry (Fig. S1), while fractions 4, 6, 8 and 21 were studied by NMR spectroscopy (Fig. S2). All fractions were left standing in open vials for slow evaporation of the solvent. From these crystallization attempts, fractions 1, 6 and 21 gave crystals. The observation that some compounds were present in nearly all fractions is most likely due to the low solubility in the eluting solvent, which led to 'smearing' over the length of the chromatography column. The use of different solvent mixtures for elution (PE/Et_2O, PE/THF and PE/CH_2Cl_2; PE is petroleum ether) increased the solubility, but did not improve the resolution of the compounds. This problem might have been overcome by the use of high-performance liquid chromatography (HPLC); however, this was not available to us.

The mass spectrum of fraction 1 showed the presence of **2** (m/z = 579.7), **3** (m/z = 659.6) and **4** (m/z = 737.5), with **2** as the main component. In both of fractions 10 and 12, **4** was the main component, contaminated by **2** (traces), **3** and **5** (m/z = 817.5). Finally, the mass spectrum of fraction 21 showed **5** as the main component, contaminated by **4** and traces of **6** (m/z = 895.2). The ^1H NMR spectra of fractions 4, 6 and 8 showed different mixtures of compounds **3** (δ = 4.47) and **4** (δ = 4.72 and 4.43) [assignments based on Butler (2021)]. The ^1H NMR spectrum of fraction 21 (in dimethyl sulfoxide) showed three very weak signals at δ = 5.33, 5.20 and 4.76, which might be assigned to **4** and **5** by comparison with the mass spectra (no other NMR data in this solvent were available). The crystals obtained from fraction 1 suffered from disorder or cocrystallization effects, which could not be properly resolved. The crystals from fraction 6 also showed disorder, which could, however, be successfully modelled as cocrystallization of compounds **3** (*ca* 97% contribution) and **2**. Fraction 21 yielded pure crystals of compound **5**.

Fig. 1 shows the structural formulae of the compounds discussed in this study.

We also repeated the permercuration of ferrocene according to Winter and co-workers, using $Hg(O_2CCH_3)_2$ as the mercurating agent and dichloroethane as the solvent, followed by bromination with KBr_3. Chromatography of the crude reaction product yielded two fractions (Han *et al.*, 1994). The first contained, according to its mass spectrum (Fig. S3), a mixture of bromoferrocenes **5**–**7** (with compound **6** dominating), while the second consisted of a mixture of bromomercurioferrocenes [$C_{10}H_nBr_{10-n}HgFe$] (n = 0–2; Fig. S4). Fig. S5 shows the ^1H NMR spectrum of the first fraction, which apparently consists of four proton-containing substances, of which one dominates. Although we did not perform these

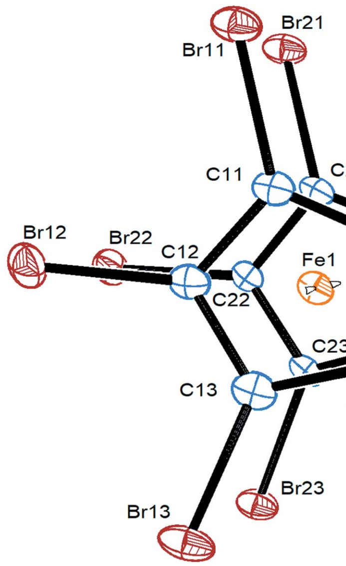

Figure 2
Top view of the molecular structure of compound **3** (major orientation), with displacement ellipsoids drawn at the 30% probability level.

experiments, it can be assumed that compounds **5–7** are formed by further bromination of $[C_{10}H_nBr_{10-n}HgFe]$. Therefore, we conclude that neither the permercuration nor the bromination reactions are complete. Although all fractions were used for crystallization attempts, only crystals of compound **8** could be obtained.

3.2. Molecular structures

An intensely debated topic since the very early days of ferrocene chemistry was the question of the relative stability of the eclipsed and staggered conformers of this molecule. While the very first crystal structure determination of ferrocene (Fischer & Pfab, 1952) hinted at a staggered geometry, the most recent low-temperature IR and XANES (X-ray absorption near edge structure) spectra, as well as DFT (density functional theory) calculations showed that the eclipsed conformation is the energy minimum (Bourke *et al.*, 2016; Silva *et al.*, 2014). For ferrocenes substituted on both rings, an additional conformational isomerism arises from the possibility of different relative positions of the substituents (Scheme 1).

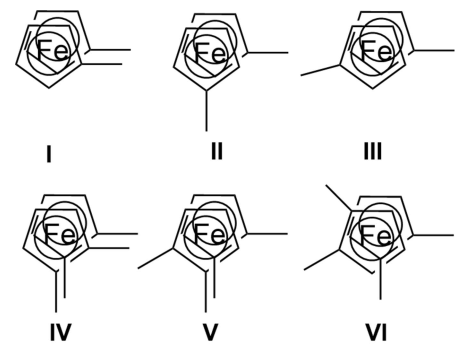

Scheme 1

While theoretical calculations on 1,1′-dibromoferrocene showed that the two C_2 isomers (**II** and **III** in Scheme 1) are minimum conformations (Silva *et al.*, 2014), in the crystal structure, only the less favourable C_{2v} structure (**I** in Scheme 1) was obtained (Hnetinka *et al.*, 2004). To obtain an overview of the 'realized' structures, a Cambridge Structural Database (CSD; Groom *et al.*, 2016) search on ferrocenes with at least one halogen substituent on each ring was undertaken. This search delivered 40 hits, of which 14 contained only halogen substituents: all four FdX_2, two FdX_3, three FdX_4, $FdCl_6$, $FdBr_9$ and $FdBr_{10}$; $FdCl_2$ was determined twice and FdI_4 exists as two positional isomers; 'Fd' is a common abbreviation for ferrocenes with substituents on both rings, while 'Fc' symbolizes ferrocenes with substituents only on one ring; strictly speaking, 'Fc' stands only for the $[C_{10}H_9Fe]$ residue, while 'Fd' symbolizes a $[(C_5H_4)_2Fe]$ group. The four 1,1′-dihaloferrocenes have been discussed already with respect to supramolecular interactions in general and halogen bonding in particular (Shimizu & Ferreira da Silva, 2018). All these

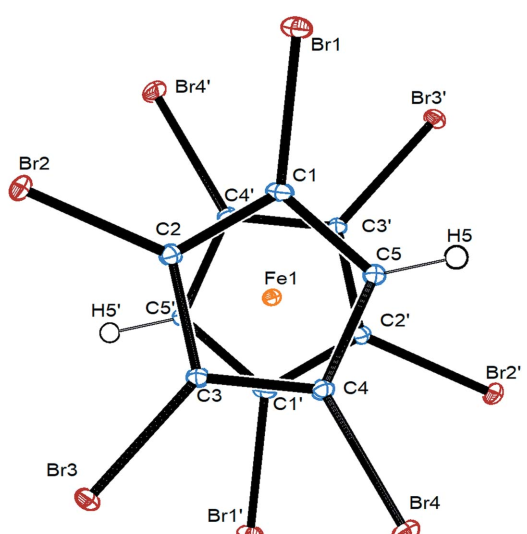

Figure 3
Top view of the molecular structure of compound **5**, showing a whole molecule, with displacement ellipsoids drawn at the 30% probability level.

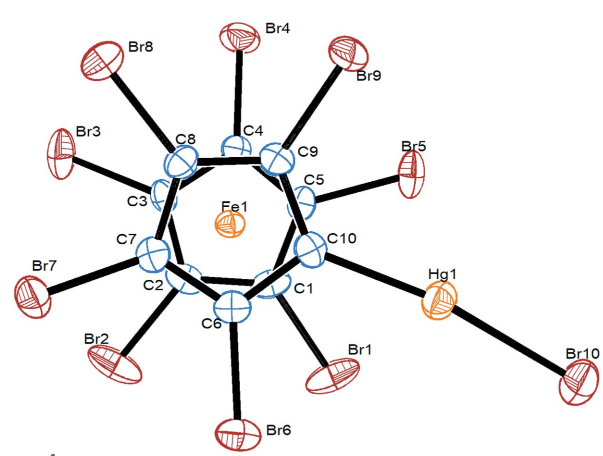

Figure 4
Top view of the molecular structure of **8**, with displacement ellipsoids drawn at the 30% probability level.

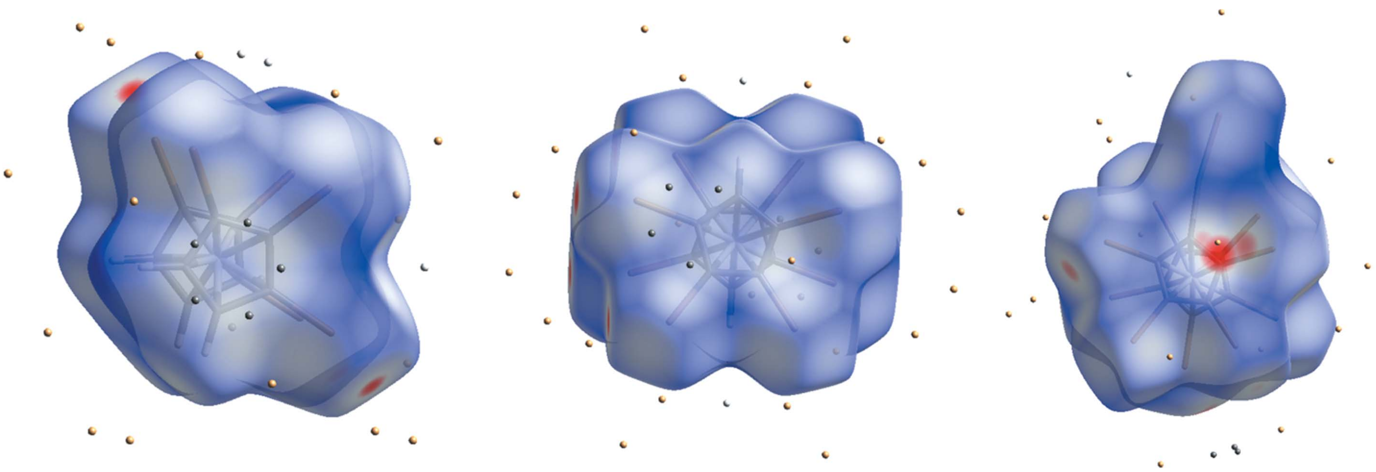

Figure 5
Hirshfeld surfaces of compounds **3** (left), **5** (middle) and **8** (right), together with the closest contact atoms. Red spots show very close contacts between atoms inside and outside the Hirshfeld surface. The Hg compound differs from the other two by the appearance of such a red spot over the plane of the Cp ring.

compounds, except for FdI_2, $FdBr_9$ and $FdBr_{10}$, showed eclipsed conformations (or nearly eclipsed in the case of $FdBr_3$ and FdI_3, with torsion angles of *ca* 14°). Within this group of eclipsed structures, most showed the apparent 'higher energy' conformations **I** and **IV**, respectively. Only $FdBr_3$, FdI_3 and FdI_4 crystallized in the most stable form **VI**. Table 2 gives an overview on these structures.

Compound **3** crystallizes in the triclinic space group $P\overline{1}$, with one molecule in the asymmetric unit. Fig. 2 shows the major orientation of the disordered molecule. As in most polyhaloferrocene structures (see Table 2), the cyclopentadienyl (Cp) rings are nearly perfectly eclipsed, planar and parallel to each other. All Br atoms are shifted slightly to the distal side of the Cp rings with respect to the Fe atom.

Compound **5** also crystallizes in the triclinic space group $P\overline{1}$, however, as a twin with half a molecule in the asymmetric unit and the Fe atom residing on an inversion centre (Fig. 3). As a consequence of this, the Cp rings are perfectly staggered, with the two C—H bonds in relative transoid positions. Both Cp rings are planar and parallel to each other and the Br atoms are all shifted to the distal sides of the Cp rings, however, to a smaller extent than in the eclipsed structures mentioned before. The iron–centroid distance (determined within *PLATON*) also seems to be more dependent on the relative orientation of the Cp rings than on the degree of bromination. Table 3 collects important geometrical parameters of several polybromoferrocenes from the literature, together with those of compounds **3**, **5** and **8**.

Compound **8** crystallizes in the monoclinic space group $P2_1/n$, with one molecule in the asymmetric unit (Fig. 4). The C10—Hg1—Br10 bond deviates slightly from being linear [171.0 (2)°]. The Cp rings are planar and parallel to each other, while their relative orientation is staggered. The distances from Fe1 to both Cp ring centroids are identical within 1σ. Except for atoms Br5 and Hg1, which are within the Cp ring planes, all the ring substituents are shifted again to the distal sides of the Cp rings. In comparison with the structure of the ferricenium salt $\mathbf{8}^{+}\cdot AsF_6^{-}$, the C—Br bonds are slightly longer,

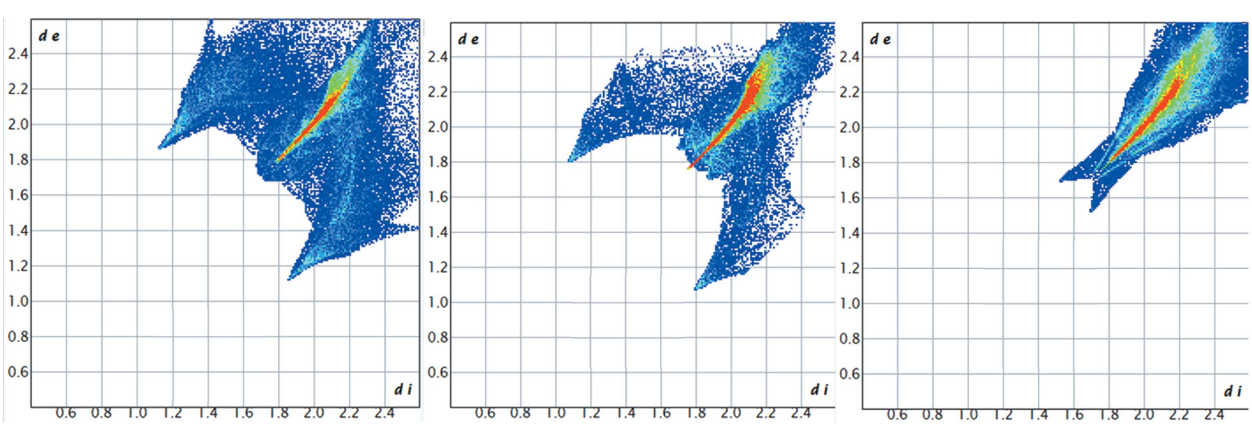

Figure 6
Fingerprint plots of compounds **3** (left), **5** (middle) and **8** (right). A red colour symbolizes a large number of points on the Hirshfeld surface at the corresponding d_e/d_i pair, green intermediate numbers and blue small numbers.

Table 3
Important geometrical parameters of compounds **3**, **5** and **8** in comparison with literature data for closely related compounds.

$FdBr_2$ is 1,1′-dibromoferrocene; 'Ct' is the abbreviation for the 'centroid' of the Cp rings, as calculated by the corresponding feature in *PLATON* (Spek, 2020); δ (Br—Cp) is the distance of the Br atoms from the Cp plane.

Compound	C—Br (Å)	Fe—C (Å)	Fe—Ct (Å)	Ct—Fe—Ct′ (°)	Br—Ct—Ct′—Br′ (°)	δ (Br—Cp) (Å)	Reference
$FdBr_2$	1.882 (4)/1.866 (4)	2.035 (4)–2.054 (4)	1.6500 (5)/1.6483 (5)	177.71 (4)	1.55 (1)	0.137 (6)/0.082 (6)	*A*
1	1.873 (2)–1.877 (2)	2.036 (2)–2.052 (2)	1.6482 (8)	177.75 (6)	1.59 (8)	0.130 (1)–0.149 (1))	*B*
3	1.862 (7)–1.881 (6)	2.033 (6)–2.064 (6)	1.653 (3)/1.654 (3)	176.3 (2)	2.09–2.38	0.123 (1)–0.168 (1)	This work
5	1.865 (3)–1.874 (3)	2.036 (6)–2.056 (3)	1.6449 (16)	180	35.9–36.2	0.037 (1)–0.096 (1)	This work
6	1.861 (10)–1.888 (11)	2.02 (1)–2.06 (1)	1.637 (1)/1.642 (1)	178.5 (3)	33.4 (5)	0.005 (1)–0.146 (1)	*C*
7	1.863 (4)–1.874 (4)	2.041 (4)–2.049 (4)	1.645 (2)	180	33.8 (2)	0.085 (1)–0.142 (1)	*C*
8	1.852 (9)–1.880 (8)	2.024 (8)–2.049 (8)	1.641 (4)/1.644 (4)	178.4 (7)	30.5 (1)–31.6 (1)	0.004 (14)–0.142 (13)	This work
$\mathbf{8}^+\cdot AsF_6$	1.845 (8)–1.865 (8)	2.066 (8)–2.116 (8)	1.703 (4)/1.708 (4)	178.9 (5)	32.5 (4)	−0.056 (1)–0.062 (1)	*C*

References: (*A*) Hnetinka *et al.* (2004); (*B*) Butler *et al.* (2021); (*C*) Rupf *et al.* (2022).

while the iron–centroid distances are significantly shorter in **8**, which is quite usual when comparing ferrocenes with their oxidized counterparts (Rupf *et al.*, 2022).

For all three compounds, an analysis with *PLATON* showed no residual solvent-accessible voids (Spek, 2020).

3.3. Hirshfeld analysis and intermolecular contacts

To gain some insight into the intermolecular interactions at work in these compounds, a Hirshfeld analysis was undertaken, using the program *CrystalExplorer* (Spackman *et al.*, 2021).

Fig. 5 shows the Hirshfeld surfaces of the three compounds, together with the closest contact atoms (within 3.8 Å).

The so-called 'fingerprint plots', which summarize all contacts between atoms inside and outside the Hirshfeld surface (Spackman & McKinnon, 2002; Spackman & Jayatilaka, 2009), are shown in Fig. 6. A common feature of all three plots is the occurrence of a red stripe around the main diagonal, reaching from *ca* d_e/d_i = 1.8/1.8 to 2.2/2.2, which corresponds to a large number of Br···Br contacts ($d_e + d_i$ = 3.6 to 4.4 Å; the sum of the van der Waals radii of two Br atoms is 3.70 Å).

The very different appearance of these plots is mainly due to the decreasing number of H atoms present. Table 4 and Fig. S8 of the supporting information provide a more detailed analysis, showing the different contributions of the individual element contacts.

Due to purely statistical effects (there are eight H atoms in $FdBr_2$, four in **3**, two in **5** and none in **8**), the absolute numbers cannot be compared directly. However, it is quite obvious that the importance of C···H and especially H···H contacts decreases drastically with increasing bromine content, while the importance of Br···Br contacts increases in the same direction. At the same time, it appears quite interesting that H···Br contacts are very important in all compounds where H atoms are present.

To obtain a more detailed picture of the individual interactions, a *Mercury* analysis was undertaken (Macrae *et al.*, 2020)

3.3.1. Hydrogen bonds. The structures of the known polyhaloferrocenes collected in Table 2 show three different

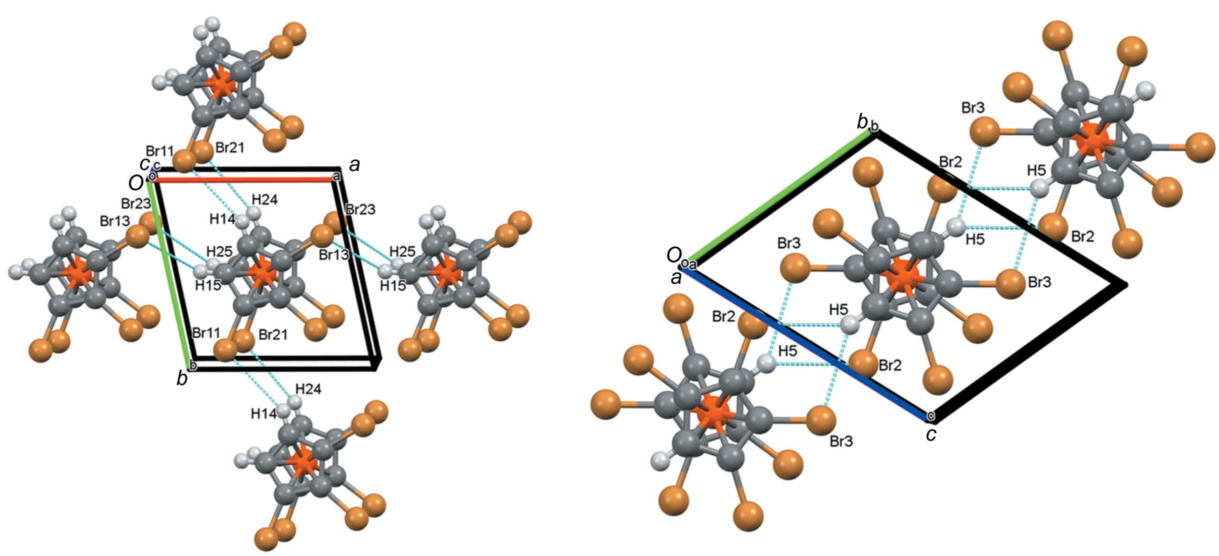

Figure 7
(Partial) packing plots (*Mercury*; Macrae *et al.*, 2020) of compounds **3** (left), viewed along *c*, and **5** (right), viewed along *a*, showing the intermolecular hydrogen bonds. Colour codes as defined by *Mercury*: carbon dark grey, hydrogen light grey, iron orange and bromine brown; the red lines are unexpanded contacts and the cyan lines are expanded contacts.

Table 4
Individual contributions (%) of the different interactions present in the crystal structures of $FdBr_2$, **3**, **5** and **8**.

Compound	C···H	C···Br	C···C	H···H	H···Br	Br···Br	Hg···Br
$FdBr_2$*	17.1	3.7	0	37.3	39.6	2.3	–
1**	6.2	1.6	6.0	14.2	52.4	19.6	–
3	3.3	4.0	5.9	0.8	48.0	38.2	–
5	1.2	6.8	5.9	0.9	20.9	64.3	
8	–	10.7	3.5	–	–	77.7	8.2

Notes: (*) taken from Shimizu & Ferreira da Silva (2018); (**) calculated from the downloaded CIF file, available from the CCDC as CSD refcode UTOBUB.

Table 5
Hydrogen-bond parameters (Å, °) in compounds **3** and **5**.

Calculated with *SHELXL2018* (Sheldrick, 2015*b*) command HTAB.

	D—H···*A*	*D*—H	H···*A*	*D*···*A*	*D*—H···*A*
3	C24—H24···Br21[i]	0.95	3.10	3.965 (9)	151.8
	C25—H25···Br23[ii]	0.95	3.13	3.874	136.5
	C14—H14···Br11[i]	0.95	3.20	4.046 (9)	149.8
	C15—H15···Br13[ii]	0.95	3.24	3.927 (8)	131.8
5	C5—H5···Br2[i]	0.95	2.985	3.786	142.93
	C5—H5···Br3[i]	0.95	3.015	3.809	141.91

patterns of hydrogen bonding (Scheme 2): Type **A** is observed in the structures of FdF_2, $FdBr_3$, FdI_3, $FdCl_4$, $FdBr_4$ and $FdBr_9$. All FdX_2, as well as iodoferrocenes and $FdBr_4$, show Type **B**, while Type **C** is seen only in the two trihaloferrocenes.

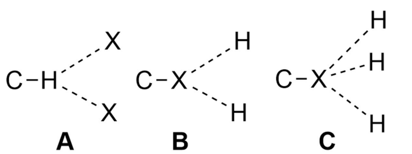

Scheme 2

When using the standard settings of *Mercury*, no hydrogen bonds are indicated for compound **3**. However, when increasing the limit by 0.2 Å, four (obviously very weak) hydrogen bonds appear [Fig. 7 (left) and Table 5].

As can be seen from Fig. 7 (left), the atom pairs H14/Br11 and H24/Br21 connect the individual molecules in the *y* direction, while the pairs H15/Br13 and H25/Br23 join them in the *x* direction. Atoms Br12 and Br22 are not involved in hydrogen bonding.

In compound **5**, the standard settings of *Mercury* suffice to show that only atom H5 (and, of course, its inversion-symmetry-generated counterpart H5′) engages in a symmetrical bifurcated hydrogen bond (Type **A** in Scheme 2) with atoms Br2 and Br3 [Fig. 7 (right) and Table 5]. As the figure shows, these interactions join individual molecules in the *y* direction.

3.3.2. Halogen bonding and other Br···Br interactions

In the discussion of halogen bonding, a distinction is usually made between XB Type I and XB Type II. According to the IUPAC and IUCr classifications, Type I contacts are geometry based, arising from close-packing requirements, while Type II arise from interactions between an electron-rich region on one halogen atom and an electron-deficient region on the other. The distinction can be made on the basis of the angles Θ1 and Θ2, which occur at halogen atoms *X* and *X*′ of *R*—*X*···*X*′—*R*′, and their difference (Scheme 3).

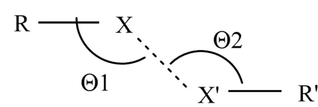

Scheme 3

Usually it is assumed that for $0 < |\Theta1 - \Theta2| < 15°$, a Type I contact is formed, while for Type II contacts, $30 < |\Theta1 - \Theta2| < 105°$ is found, and only the latter are regarded as real halogen bonds (Cavallo *et al.*, 2016). In a more recent article, a distinction into Types I–IV was suggested, but was still based on these angles (Ibrahim *et al.*, 2022): Type I: $90 < \Theta1 \simeq \Theta2 < 180°$; Type II: $\Theta1 = 180°$ and $\Theta2 = 90°$; Type III: $\Theta1 \simeq \Theta2 = 180°$; Type IV: $\Theta1 \simeq \Theta2 = 90°$ (obviously, Types III and IV are only extrema of the more general Type I). The forces behind these attractions are either van der Waals (Type I), electrostatic (Type II) or dispersion (Types III and IV) forces. It was further found that 'the Type I interactions were more frequent at the shortest distances' (Cavallo *et al.*, 2016). Table 6 collects

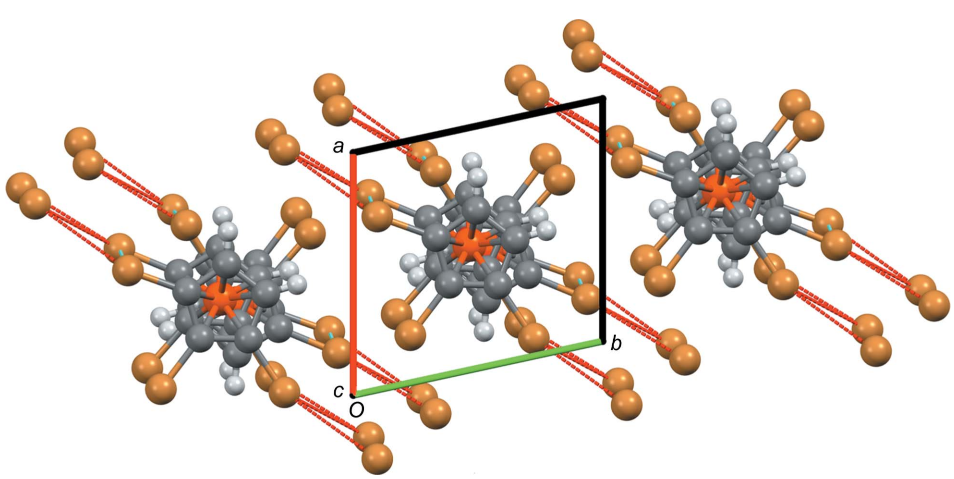

Figure 8
Packing plot of compound **3**, viewed along *c*. Colour codes as defined by *Mercury*: carbon dark grey, hydrogen light grey, iron orange and bromine brown; the red lines are unexpanded contacts and the cyan lines are expanded contacts.

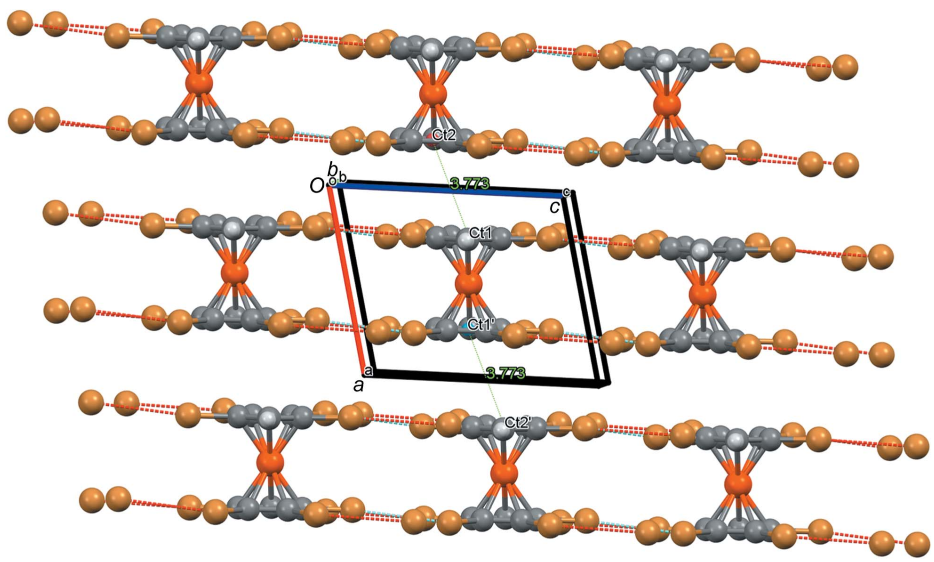

Figure 9
Packing plot of compound **5**, viewed along *b*. Colour codes as defined by *Mercury*: carbon dark grey, hydrogen light grey, iron orange and bromine brown; the red lines are unexpanded contacts and the cyan lines are expanded contacts.

the structural parameters of compounds **3**, **5** and **8**, while Figs. S9–S11 show *Mercury* representations of these interactions.

All the listed Br···Br contacts in Table 6 are well below the sum of the van der Waals radii (3.70 Å; Bondi, 1964). When using the |Θ1 − Θ2| criterion, most interactions classified as Type II are also 'real' halogen bonds. To look at the structural consequences of this halogen bonding, a visualization of the packing plots should be helpful.

Fig. 8 shows how the Br···Br interactions join the individual molecules of compound **3** in the direction of the *xy* diagonal (*b*–*a* vector). It can also be seen that there are two *intra*molmolecular Br···Br contacts of Type IV, emphasized in italic in Table 5. Two Br atoms (Br12 and Br22) are not involved in Br···Br interactions. Fig. 9 shows that in compound **5** the Br···Br contacts join the individual molecules in the *z* direction. All eight Br atoms are involved in Br···Br interactions. In addition, there is also some π–π stacking in the *x* direction; the centroids of two adjacent Cp rings are only 3.773 Å apart, while the ring planes have an interplanar distance of 3.507 Å (corresponding to an angle of 21.6° between the Ct—Ct′ vector and the plane normal).

In bromomercurio compound **8**, matters are a bit more complicated. Fig. 10 shows that Br···Br contacts join the individual molecules in all directions. All Br atoms, except for Br2, Br5 and Br8, are involved in Br···Br contacts.

But there are more interactions involving Br atoms. First there are Hg···Br contacts, shown in Fig. 11. The Hg1···Hg1 distance is 4.4944 (6) Å and therefore any mercurophilic

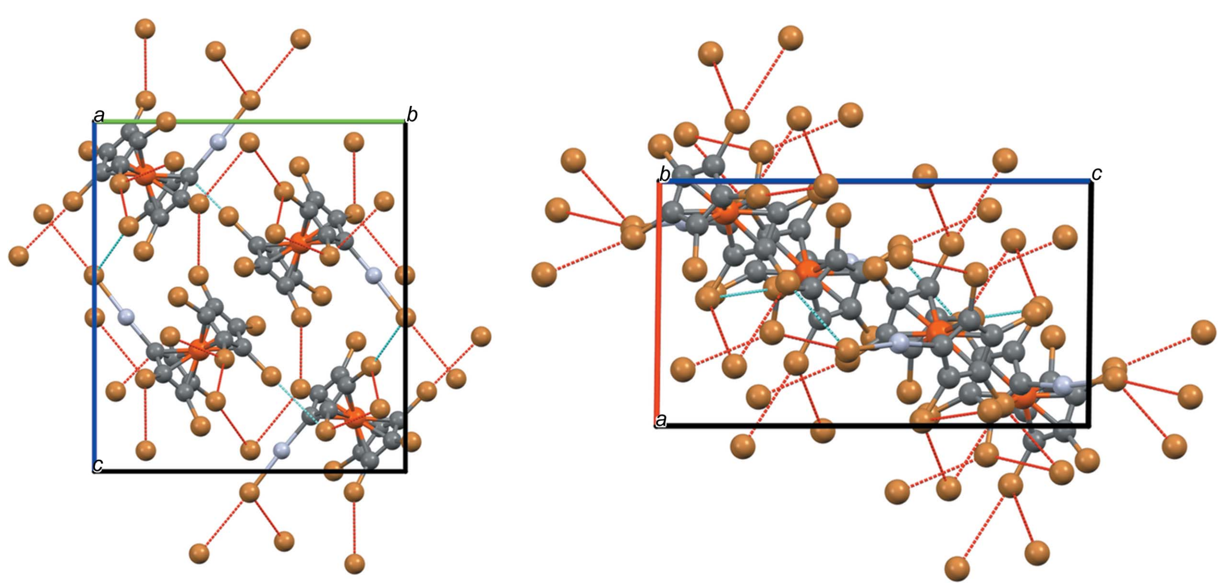

Figure 10
Packing plots of compound **8**, viewed along *a* (left) and along *b* (right). Colour codes as defined by *Mercury*: carbon dark grey, hydrogen light grey, iron orange and bromine brown; the red lines are unexpanded contacts and the cyan lines are expanded contacts.

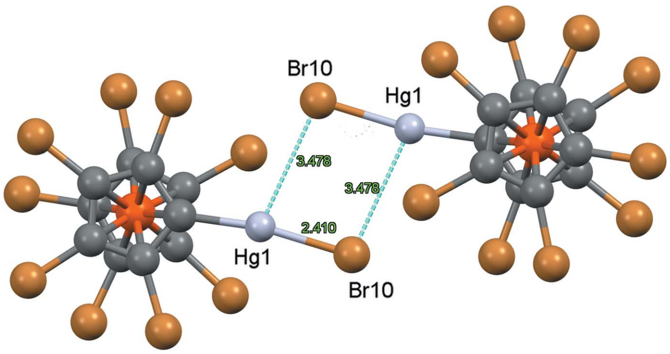

Figure 11
The Hg_2Br_2 ring in compound **8**. Colour codes as defined by *Mercury*: carbon dark grey, hydrogen light grey, iron orange and bromine brown; the red lines are unexpanded contacts and the cyan lines are expanded contacts. Generic atom labels without symmetry codes ahve been used.

interactions (Schmidbaur & Schier, 2015) can be excluded. In the crystal of the ferricenium complex $\mathbf{8}^{+}\cdot AsF_6^{-}$, there is also a Hg_2Br_2 ring with significantly shortened intermolecular Hg···Br contacts of 3.061 Å and a Hg···Hg distance of 3.993 Å (Rupf *et al.*, 2022). Furthermore, there are Br···π contacts of 3.543 Å to a close Cp ring, in addition to a weak π–π interaction between two Cp rings (Fig. 12); π–π stacking occurs between two inversion-related C_5Br_5 rings. Since the difference between the Ct—Ct′ distance of 3.756 Å and the perpendicular distance between the Cp ring planes (3.690 Å) is rather small (corresponding to an angle of 10.8° between the Ct—Ct′ vector and the plane normal), it can be regarded as a 'true' π–π interaction (though rather weak).

A similar Br···π interaction was found in the structure of $FdBr_2$; however, it was, with a Br···centroid distance of 3.824 Å, substantially weaker (Shimizu & Ferreira da Silva, 2018).

3.3.3. Co-operativity between H···Br and Br···Br contacts. The importance of co-operativity in noncovalent interactions in general (Mahadevi & Sastry, 2016) and for the interplay of halogen and hydrogen bonds (Decato *et al.*, 2021; Portela & Fernández, 2021) in particular has been recognized in recent years and has been modelled by DFT calculations. This interplay has also been discussed for the 1,1′-dihaloferrocenes (Shimizu & Ferreira da Silva, 2018). In the preceding sections, we have discussed the individual contributions in compounds **3** and **5**, and a look at Fig. 13 (and Tables 4 and 5) shows that also in these compounds HB and XB work together on the same halogen atoms.

3.3.4. Energetics of the intermolecular interactions found in compounds 3, 5 and 8. The program *CrystalExplorer* allows for the calculation of interaction energies using the DFT program *TONTO* at the HF/3-21G level (Mackenzie *et al.*, 2017). Fig. 14 shows the results of calculations for compounds **3** and **5** (apparently, due to the presence of Hg, the program cannot calculate wavefunctions for compound **8**).

Inspection of the numerical values shows that the total interaction energies are stronger for compound **3**. This is apparently due to the larger repulsion terms for **5**, because both the largest dispersion and the largest electrostatic terms are found in compound **5**. Another graphical representation ('energy frameworks') of the individual contributions can be seen in Fig. 15.

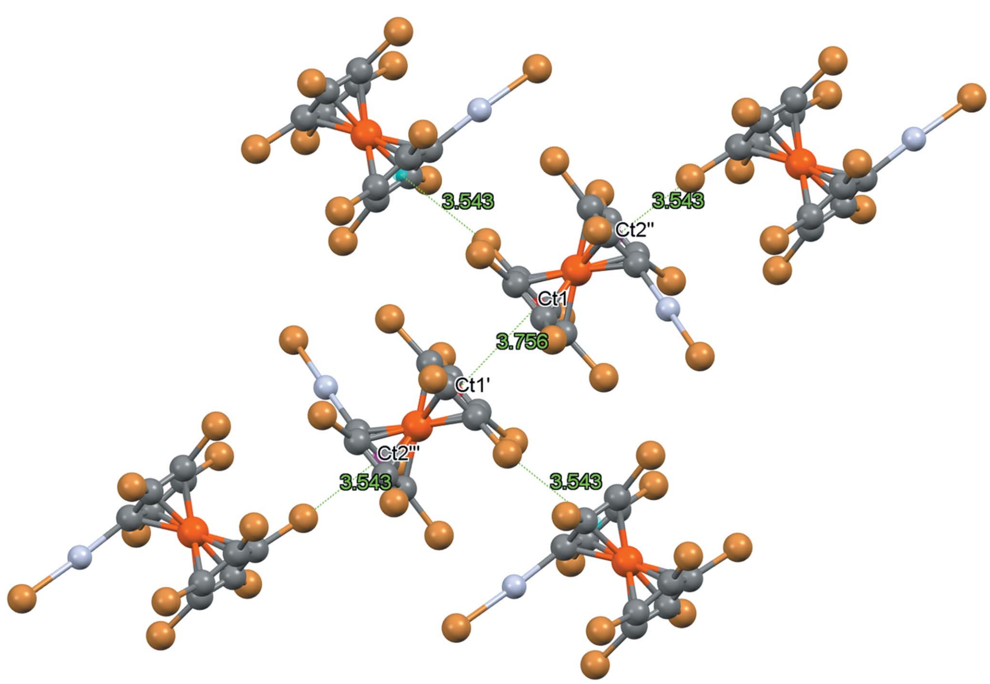

Figure 12
Partial packing diagram of compound **8**, showing the Br···π and π–π contacts (Å). Colour codes as defined by *Mercury*: carbon dark grey, hydrogen light grey, iron orange, mercury blue and bromine brown; the red lines are unexpanded contacts and the cyan lines are expanded contacts. Ct1′/Ct1″ and Ct2′/Ct2″ are the centroids of inversion-related cyclopentadienyl rings, with one Fe atom between Ct1′ and Ct2′, and another between Ct1″ and Ct2″.

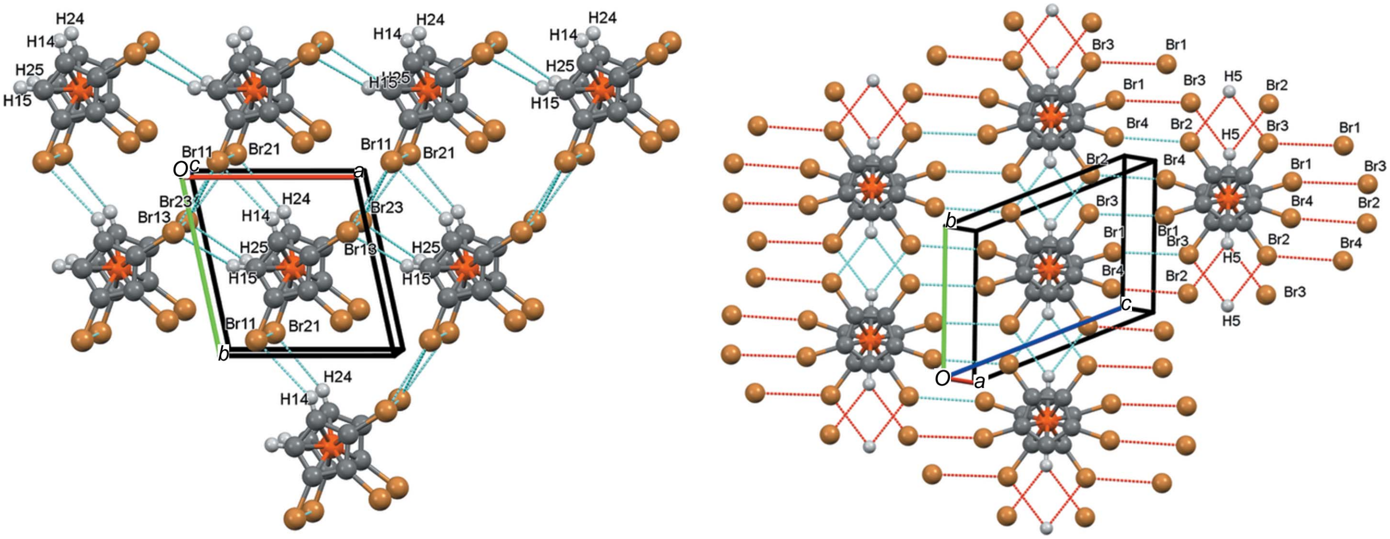

Figure 13
Co-operativity of hydrogen and halogen bonding in compounds **3** and **5**. Colour codes as defined by *Mercury*: carbon dark grey, hydrogen light grey, iron orange and bromine brown; the red lines are unexpanded contacts and the cyan lines are expanded contacts.

3.3.5. Comparison with halogen bonding in other haloferrocenes FdX_n with $X \neq$ Br and $n > 2$. At this point, it seems worthwhile to look at the occurrence of halogen bonding in the other polyhaloferrocenes mentioned in Table 2. As mentioned already, this study has been performed for the 1,1′-dihaloferrocenes before, and therefore these structures will

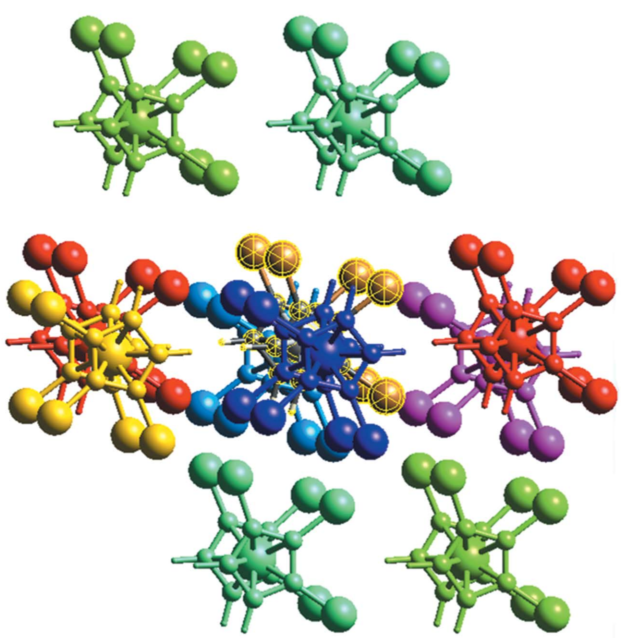

	N	Symop	R	Electron Density	E_ele	E_pol	E_dis	E_rep	E_tot
(red)	2	x, y, z	7.09	HF/3-21G	-11.7	-2.7	-40.6	24.1	-30.7
(yellow)	1	-x, -y, -z	10.86	HF/3-21G	-0.4	-0.4	-2.7	-0.0	-3.1
(green)	2	x, y, z	9.12	HF/3-21G	-6.4	-0.2	-17.5	22.2	-4.5
(light green)	2	x, y, z	7.43	HF/3-21G	-7.9	-2.2	-28.3	12.3	-25.1
(light blue)	1	-x, -y, -z	7.41	HF/3-21G	-6.6	-2.3	-48.2	27.5	-29.4
(dark blue)	1	-x, -y, -z	7.30	HF/3-21G	-10.0	-2.8	-55.1	30.2	-37.2
(purple)	1	-x, -y, -z	8.58	HF/3-21G	-1.2	-0.4	-16.0	10.1	-7.7

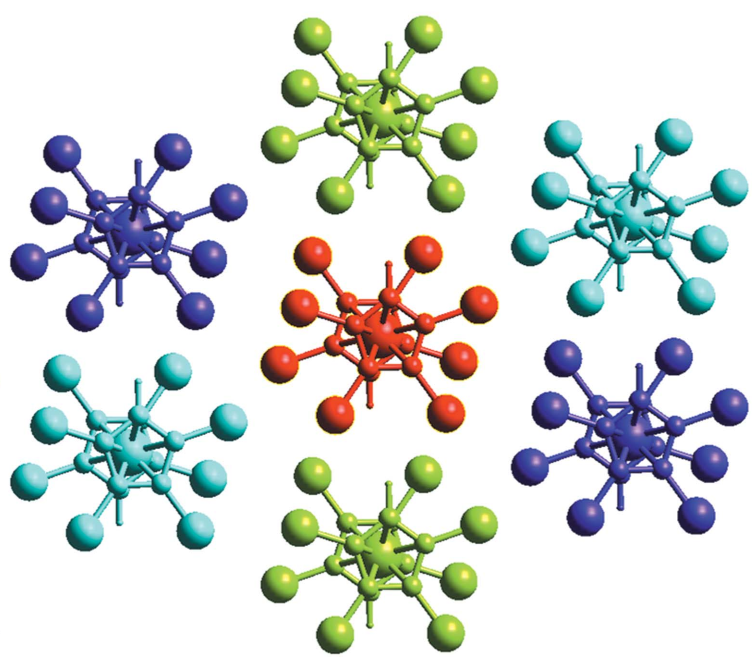

	N	Symop	R	Electron Density	E_ele	E_pol	E_dis	E_rep	E_tot
(red)	2	x, y, z	6.94	HF/3-21G	-8.8	-1.2	-64.2	33.2	-40.7
(green)	2	x, y, z	7.05	HF/3-21G	-20.1	-1.9	-53.5	48.1	-30.8
(cyan)	2	x, y, z	9.02	HF/3-21G	-5.8	-0.4	-21.2	17.4	-11.2
(blue)	2	x, y, z	8.93	HF/3-21G	-8.2	-0.5	-23.6	22.3	-11.9

Figure 14
Interaction energies (HF/3-21G) for compounds **3** (left) and **5** (right) (standard program settings). The colour codes in the images refer to the tables below them.

Table 6
Characteristics of the Br···Br interactions found in compounds **1**, **3**, **5**, **8** and $FdBr_2$.

Compound	R—Br···Br′—$R′$	Br···Br (Å)	Θ1 (°)	Θ2 (°)	|Θ1 − Θ2| (°)	XB Type
$FdBr_2$*	C1—Br1···Br2—C6	3.586	89.7	153.1	63.2	II
1**	C1—Br1···Br2—C2	3.564	145.2	156.4	11.2	I
3	C13—Br13···Br11—C11	3.617	135.2	153.8	18.6	Quasi-Type I/Type II
	C23—Br23···Br11—C11	3.582	137.3	143.3	6.0	I
	C23—Br23···Br21—C21	3.594	146.9	141.8	5.1	I
	C13—Br13···Br23—C23	*3.656*	*84.7*	*85.1*	*0.4*	IV
	C11—Br11···Br21—C21	*3.657*	*85.2*	*84.4*	*0.8*	IV
5	C1—Br1···Br3—C3	3.518	160.8	124.8	36.0	II
	C2—Br2···Br4—C4	3.538	128.9	163.8	34.9	II
8	C1—Br1···Br9—C9	3.545	154.8	117.4	37.4	II
	C4—Br4···Br6—C6	3.634	117.7	113.1	4.6	I
	C4—Br4···Br7—C7	3.657	171.4	112.5	58.9	II
	C3—Br3···Br6—C6	3.521	174.1	65.9	108.2	II
	C7—Br7···Br10—Hg1	3.658	167.0	97.9	69.1	II
	C9—Br9···Br10—Hg1	3.642	109.4	163.4	54.0	II

Notes: (*) taken from Shimizu & Ferreira da Silva (2018); (**) calculated from the downloaded CIF file, available from the CCDC as CSD refcode UTOBUB.

not be considered here again. Instead, the structure of the homoannularly substituted pentabromoferrocene ($FcBr_5$; Sünkel & Bernhartzeder, 2011) is included (Table 7). All the listed $X\cdots X$ contacts are below the sum of the van der Waals radii and of Type II except for the chloro compound (0.004 Å longer than this sum and Type I). This result (the increasing importance of $X\cdots X$ contacts when going from X = Cl to X = I) parallels the observations in the FdX_2 sytems. In addition to the $X\cdots X$ interactions, C—H···X hydrogen bonds are important for all compounds, especially the chloro compound. π–π interactions are very strong for FdI_4 (virtually no displacement of the Cp rings of different molecules), while in $FdCl_4$, the shift between the perpendicular projection of one centroid to the centroid of a neighbouring molecule is quite substantial. In FdI_3, C—H···π interactions seem to be of some importance, while in $FcBr_5$, a weak C—Br···π interaction can be observed.

4. Conclusion

Both stepwise deprotonation/electrophilic bromination starting from 1,1′,2,2′-tetrabromoferrocene and permercuration/bromination of ferrocene lead to mixtures of polybrominated ferrocenes. However, by a combination of chromatography and recrystallization, it was possible to obtain crystals of hexa- and octabromoferrocene, as well as of nonabromo(bromomercur-

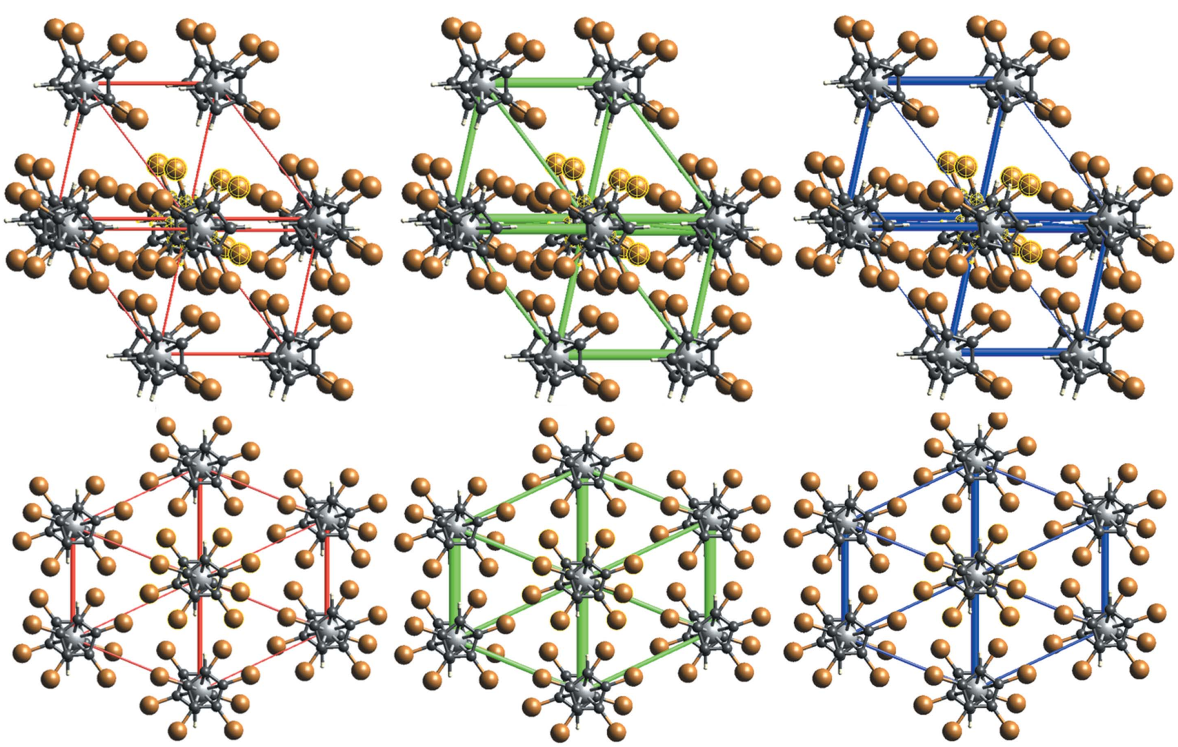

Figure 15
Energy frameworks (Coulombic energy in red, dispersion energy in green and total energy in blue) for compounds **3** (top) and **5** (bottom).

Table 7
Characteristics of the $X\cdots X$ interactions in $FdCl_4$, FdI_3, FdI_4 and $FcBr_5$.

	$R-X\cdots X'-R'$	$X\cdots X$ (Å)	Θ1 (°)	Θ2 (°)	|Θ1 − Θ2| (°)	XB Type
FdI_3	C1−I1···Br2−C2	3.74p	90.5	172.6	82.1	II
	C1−I1···I3−C6	3.728	174.4	115.1	59.3	II
FdI_4	C1−I1···I3−C6	3.679	165.1	79.9	85.2	II
	C2−I2···I12−C12	3.933	159.6	97.1	62.5	II
	C6−I3···I13−C16	3.756	99.4	169.3	69.9	II
	C7−I4···I12−C12	3.823	83.0	165.8	82.8	II
	C11−I11···I13−C16	3.823	163.0	70.3	92.7	II
$FdCl_4$	C11−Cl1···Cl2−C21	3.504	165.5	161.5	4.0	I
$FcBr_5$	C2*A*−Br2*A*···Br3*B*−C3*B*	3.352	137.3	168.4	31.1	II
	C2*B*−Br2*B*···Br3*B*−C3*B*	3.656	164.7	123.2	41.5	II

io)ferrocene. Hexabromoferrocene shows an eclipsed conformation of the Cp rings, as was also found for the already known structures of 1,1′-dibromo- and 1,1′,2,2′-tetrabromoferrocene. Ferrocenes with a higher bromine content apparently prefer a staggered conformation, as was observed before for nona- and decabromoferrocene. All three title compounds show a combination of halogen bonding with either hydrogen bonding or π–π interactions. Dispersion interactions appear to be stronger than electrostatic interactions.

Acknowledgements

Open access funding enabled and organized by Projekt DEAL.

References

Agilent (2014). *CrysAlis PRO*. Agilent Technologies Ltd, Yarnton, Oxfordshire, England.
Boev, V. I. & Dombrovskii, A. V. (1977). *Zh. Obshch. Khim.* **47**, 727–728.
Bondi, A. (1964). *J. Phys. Chem.* **68**, 441–451.
Bourke, J. D., Islam, M. T., Best, S. P., Tran, C. Q., Wang, F. & Chantler, C. T. (2016). *J. Phys. Chem. Lett.* **7**, 2792–2796.
Brammer, L., Mínguez Espallargas, G. & Libri, S. (2008). *CrystEngComm*, **10**, 1712–1727.
Bruker (2011). *APEX2* and *SAINT*. Bruker AXS Inc., Madison, Wisconsin, USA.
Bruker (2012). *APEX2*, *SAINT* and *TWINABS*. Bruker AXS Inc., Madison, Wisconsin, USA.
Bryan, R. F. & Leadbetter, A. J. (1986). American Crystallographic Association, Abstracts (Winter), **14**, 28b.
Butenschön, H. (2018). *Synthesis*, **50**, 3787–3808.
Butler, I. R. (2021). *Organometallics*, **40**, 3240–3244.
Butler, I. R., Beaumont, M., Bruce, M. I., Zaitseva, N. N., Iggo, J. A., Robertson, C., Horton, P. N. & Coles, S. J. (2021). *Aust. J. Chem.* **74**, 204–210.
Cavallo, G., Metrangolo, P., Milani, R., Pilati, T., Priimagi, A., Resnati, G. & Terraneo, G. (2016). *Chem. Rev.* **116**, 2478–2601.
Decato, D. A., Riel, A. M. S., May, J. H., Bryantsev, V. S. & Berryman, O. B. (2021). *Angew. Chem. Int. Ed.* **60**, 3685–3692.
Evans, D. M., Hughes, D. D., Murphy, P. J., Horton, P. N., Coles, S. J., de Biani, F. F., Corsini, M. & Butler, I. R. (2021). *Organometallics*, **40**, 2496–2503.
Fischer, E. O. & Pfab, W. (1952). *Z. Naturforsch.* **7**, 377–379.
Groom, C. R., Bruno, I. J., Lightfoot, M. P. & Ward, S. C. (2016). *Acta Cryst.* B**72**, 171–179.
Han, Y.-H., Heeg, M. J. & Winter, C. H. (1994). *Organometallics*, **13**, 3009–3019.
Hnetinka, C. A., Hunter, A. D., Zeller, M. & Lesley, M. J. G. (2004). *Acta Cryst.* E**60**, m1806–m1807.
Hobza, P. & Řezáč, J. (2016). *Chem. Rev.* **116**, 4911–4912.
Ibrahim, M. A. A., Saeed, R. R. A., Shehata, M. N. I., Ahmed, M. N., Shawky, A. M., Khowdiary, M. M., Elkaeed, E. B., Soliman, M. E. S. & Moussa, N. A. M. (2022). *Int. J. Mol. Sci.* **23**, 3114–3130.
Inkpen, M. S., Du, S., Hildebrand, M., White, A. J. P., Harrison, N. M., Albrecht, T. & Long, N. J. (2015). *Organometallics*, **34**, 5461–5469.
Kelly, A. W. & Holman, K. T. (2022). *Angew. Chem. Int. Ed.* **61**, e202115556.
Krause, L., Herbst-Irmer, R., Sheldrick, G. M. & Stalke, D. (2015). *J. Appl. Cryst.* **48**, 3–10.
Mackenzie, C. F., Spackman, P. R., Jayatilaka, D. & Spackman, M. A. (2017). *IUCrJ*, **4**, 575–587.
Macrae, C. F., Sovago, I., Cottrell, S. J., Galek, P. T. A., McCabe, P., Pidcock, E., Platings, M., Shields, G. P., Stevens, J. S., Towler, M. & Wood, P. A. (2020). *J. Appl. Cryst.* **53**, 226–235.
Mahadevi, A. S. & Sastry, G. N. (2016). *Chem. Rev.* **116**, 2775–2825.
Mukherjee, A., Tothadi, S. & Desiraju, G. R. (2014). *Acc. Chem. Res.* **47**, 2514–2524.
Neto, A. F., Borges, A. D. L., de Arruda Campos, P. & Miller, J. (1997). *Synth. React. Inorg. Met.-Org. Chem.* **27**, 1543–1551.
Portela, S. & Fernández, I. (2021). *Molecules*, **26**, 1885–1894.
Roemer, M. & Nijhuis, C. A. (2014). *Dalton Trans.* **43**, 11815–11818.
Rupf, S. M., Dimitrova, I. S., Schröder, G. & Malischewski, M. (2022). *Organometallics*, **41**, 1261–1267.
Sato, K., Konno, M. & Sano, H. (1984). *Chem. Lett.* **13**, 17–20.
Schmidbaur, H. & Schier, A. (2015). *Organometallics*, **34**, 2048–2066.
Sheldrick, G. M. (2015*a*). *Acta Cryst.* A**71**, 3–8.
Sheldrick, G. M. (2015*b*). *Acta Cryst.* C**71**, 3–8.
Shimizu, K. & Ferreira da Silva, J. (2018). *Molecules*, **23**, 2959–2977.
Silva, P. A., Maria, T. M. R., Nunes, C. M., Eusébio, M. E. S. & Fausto, R. (2014). *J. Mol. Struct.* **1078**, 90–105.
Spackman, M. A. & Jayatilaka, D. (2009). *CrystEngComm*, **11**, 19–32.
Spackman, M. A. & McKinnon, J. J. (2002). *CrystEngComm*, **4**, 378–392.
Spackman, P. R., Turner, M. J., McKinnon, J. J., Wolff, S. K., Grimwood, D. J., Jayatilaka, D. & Spackman, M. A. (2021). *J. Appl. Cryst.* **54**, 1006–1011.
Spek, A. L. (2020). *Acta Cryst.* E**76**, 1–11.
Sünkel, K. & Bernhartzeder, S. (2011). *J. Organomet. Chem.* **696**, 1536–1540.
Sünkel, K. & Hofmann, J. (1992). *Organometallics*, **11**, 3923–3925.
Sünkel, K., Kempinger, W. & Hofmann, J. (1994). *J. Organomet. Chem.* **475**, 201–209.
Sünkel, K. & Motz, D. (1988). *Angew. Chem. Int. Ed. Engl.* **27**, 939–941.
Sünkel, K., Weigand, S., Hoffmann, A., Blomeyer, S., Reuter, C. G., Vishnevskiy, Y. V. & Mitzel, N. (2015). *J. Am. Chem. Soc.* **137**, 126–129.

supporting information

Acta Cryst. (2022). C**78**, 578-590 [https://doi.org/10.1107/S205322962200955X]

Isolation and crystal and molecular structures of [($C_5H_2Br_3$)$_2$Fe], [(C_5HBr_4)$_2$Fe] and [(C_5Br_5)(C_5Br_4HgBr)Fe]

Tobias Blockhaus and Karlheinz Sünkel

Computing details

Data collection: *CrysAlis PRO* (Agilent, 2014) for compd_3; *APEX2* (Bruker, 2012) for compd_5, compd_8. Cell refinement: *CrysAlis PRO* (Agilent, 2014) for compd_3; *APEX2* (Bruker, 2012) for compd_5, compd_8. Data reduction: *CrysAlis PRO* (Agilent, 2014) for compd_3; *SAINT* (Bruker, 2011) for compd_5, compd_8. Program(s) used to solve structure: SHELXT (Sheldrick, 2015*a*) for compd_3, compd_5; SHELXT2014 (Sheldrick, 2015*a*) for compd_8. For all structures, program(s) used to refine structure: *SHELXL2018* (Sheldrick, 2015*b*).

Bis(1,2,3-tribromocyclopentadienyl)iron(II) (compd_3)

Crystal data

[Fe($C_5H_2Br_3$)$_2$]
M_r = 656.69
Triclinic, $P\overline{1}$
a = 7.0903 (3) Å
b = 7.4318 (5) Å
c = 13.8071 (5) Å
α = 88.745 (4)°
β = 84.993 (3)°
γ = 77.728 (4)°
V = 708.21 (6) Å^3
Z = 2
F(000) = 598
D_x = 3.079 Mg m^{-3}
Mo $K\alpha$ radiation, λ = 0.71073 Å
Cell parameters from 2222 reflections
θ = 4.4–29.1°
μ = 17.86 mm^{-1}
T = 153 K
Rod, yellow
0.49 × 0.15 × 0.05 mm

Data collection

Agilent XCalibur 2 diffractometer
Radiation source: Enhance (Mo) X-ray Source
Graphite monochromator
Detector resolution: 15.9809 pixels mm^{-1}
ω scans
Absorption correction: multi-scan (CrysAlis PRO; Agilent, 2014)
T_{min} = 0.434, T_{max} = 1.000
9297 measured reflections
3234 independent reflections
2496 reflections with $I > 2\sigma(I)$
R_{int} = 0.041
θ_{max} = 27.5°, θ_{min} = 4.4°
h = −9→9
k = −9→9
l = −17→17

Refinement

Refinement on F^2
Least-squares matrix: full
$R[F^2 > 2\sigma(F^2)]$ = 0.043
$wR(F^2)$ = 0.090
S = 1.09
3234 reflections
162 parameters
2 restraints
Primary atom site location: dual
Hydrogen site location: inferred from neighbouring sites
H-atom parameters constrained
$w = 1/[\sigma^2(F_o^2) + (0.0263P)^2 + 2.1323P]$ where $P = (F_o^2 + 2F_c^2)/3$

$(\Delta/\sigma)_{max} = 0.001$
$\Delta\rho_{max} = 2.31$ e Å^{-3}
$\Delta\rho_{min} = -0.97$ e Å^{-3}

Special details

Geometry. All e.s.d.'s (except the e.s.d. in the dihedral angle between two l.s. planes) are estimated using the full covariance matrix. The cell e.s.d.'s are taken into account individually in the estimation of e.s.d.'s in distances, angles and torsion angles; correlations between e.s.d.'s in cell parameters are only used when they are defined by crystal symmetry. An approximate (isotropic) treatment of cell e.s.d.'s is used for estimating e.s.d.'s involving l.s. planes.

Fractional atomic coordinates and isotropic or equivalent isotropic displacement parameters (Å^2)

	x	y	z	U_{iso}*/U_{eq}	Occ. (<1)
Br11	0.18791 (10)	0.93782 (10)	0.66385 (5)	0.03293 (18)	0.964
Br12	0.70467 (10)	0.82612 (11)	0.59801 (5)	0.0373 (2)	0.964
Br13	0.85028 (10)	0.33022 (11)	0.57625 (4)	0.0392 (2)	
Br21	0.28443 (10)	0.90368 (10)	0.92101 (5)	0.03273 (18)	0.962
Br22	0.80318 (10)	0.77138 (11)	0.86137 (5)	0.03604 (18)	
Br23	0.92650 (9)	0.27609 (10)	0.83466 (5)	0.03364 (18)	
Br14	0.434 (2)	0.195 (3)	0.6369 (13)	0.035 (4)*	0.036
Br24	0.468 (2)	0.154 (3)	0.8634 (13)	0.034 (4)*	0.038
Fe1	0.48302 (12)	0.53419 (13)	0.75694 (6)	0.0237 (2)	
C11	0.3423 (9)	0.7001 (9)	0.6536 (4)	0.0261 (14)	
H11	0.264311	0.820193	0.663236	0.031*	0.036
C12	0.5467 (9)	0.6582 (9)	0.6273 (4)	0.0271 (15)	
H12	0.628980	0.743553	0.616656	0.033*	0.036
C13	0.6018 (9)	0.4628 (9)	0.6202 (4)	0.0284 (15)	
C14	0.4345 (10)	0.3851 (10)	0.6407 (4)	0.0326 (16)	
H14	0.430543	0.258235	0.639497	0.039*	0.964
C15	0.2755 (10)	0.5343 (10)	0.6631 (4)	0.0317 (16)	
H15	0.145828	0.524053	0.681342	0.038*	
C21	0.4231 (8)	0.6678 (9)	0.8879 (4)	0.0259 (14)	
H21	0.351021	0.789982	0.898573	0.031*	0.038
C22	0.6274 (9)	0.6154 (9)	0.8647 (4)	0.0237 (13)	
C23	0.6743 (8)	0.4208 (9)	0.8548 (4)	0.0233 (14)	
C24	0.5032 (10)	0.3515 (10)	0.8713 (4)	0.0332 (16)	
H24	0.493556	0.226119	0.868992	0.040*	0.962
C25	0.3465 (9)	0.5074 (10)	0.8921 (4)	0.0293 (15)	
H25	0.214046	0.502975	0.906335	0.035*	

Atomic displacement parameters (Å^2)

	U^{11}	U^{22}	U^{33}	U^{12}	U^{13}	U^{23}
Br11	0.0307 (4)	0.0358 (4)	0.0253 (3)	0.0076 (3)	−0.0012 (3)	0.0037 (3)
Br12	0.0340 (4)	0.0432 (5)	0.0328 (4)	−0.0084 (3)	0.0071 (3)	0.0079 (3)
Br13	0.0371 (4)	0.0508 (5)	0.0200 (3)	0.0122 (3)	−0.0003 (3)	−0.0041 (3)
Br21	0.0323 (4)	0.0359 (4)	0.0232 (3)	0.0067 (3)	0.0014 (3)	−0.0041 (3)
Br22	0.0313 (4)	0.0408 (4)	0.0375 (4)	−0.0107 (3)	−0.0017 (3)	−0.0080 (3)
Br23	0.0294 (4)	0.0380 (4)	0.0277 (3)	0.0063 (3)	−0.0045 (3)	0.0020 (3)
Fe1	0.0240 (5)	0.0314 (5)	0.0143 (4)	−0.0022 (4)	−0.0029 (3)	0.0016 (4)

C11	0.028 (3)	0.031 (4)	0.016 (3)	0.002 (3)	−0.003 (2)	0.003 (3)
C12	0.031 (3)	0.031 (4)	0.016 (3)	0.000 (3)	−0.001 (3)	−0.001 (3)
C13	0.032 (3)	0.036 (4)	0.015 (3)	−0.002 (3)	−0.004 (3)	−0.003 (3)
C14	0.040 (4)	0.038 (4)	0.021 (3)	−0.010 (3)	−0.008 (3)	−0.004 (3)
C15	0.030 (4)	0.047 (5)	0.021 (3)	−0.014 (3)	−0.009 (3)	0.007 (3)
C21	0.019 (3)	0.033 (4)	0.021 (3)	0.002 (3)	0.001 (2)	0.004 (3)
C22	0.023 (3)	0.033 (4)	0.015 (3)	−0.005 (3)	−0.003 (2)	−0.001 (3)
C23	0.018 (3)	0.037 (4)	0.013 (3)	−0.001 (3)	−0.003 (2)	0.001 (3)
C24	0.044 (4)	0.037 (4)	0.018 (3)	−0.007 (3)	−0.006 (3)	0.006 (3)
C25	0.024 (3)	0.045 (4)	0.017 (3)	−0.003 (3)	−0.003 (2)	0.002 (3)

Geometric parameters (Å, º)

Br11—C11	1.871 (6)	C11—C15	1.411 (9)
Br12—C12	1.862 (7)	C11—C12	1.432 (9)
Br13—C13	1.883 (6)	C11—H11	0.9500
Br21—C21	1.863 (6)	C12—C13	1.424 (9)
Br22—C22	1.871 (7)	C12—H12	0.9500
Br23—C23	1.881 (6)	C13—C14	1.430 (9)
Br14—C14	1.41 (2)	C14—C15	1.421 (9)
Br24—C24	1.55 (2)	C14—H14	0.9500
Fe1—C13	2.033 (6)	C15—H15	0.9500
Fe1—C23	2.039 (6)	C21—C25	1.409 (9)
Fe1—C15	2.044 (6)	C21—C22	1.427 (8)
Fe1—C22	2.048 (6)	C21—H21	0.9500
Fe1—C11	2.049 (6)	C22—C23	1.420 (9)
Fe1—C21	2.049 (6)	C23—C24	1.415 (9)
Fe1—C25	2.052 (6)	C24—C25	1.439 (9)
Fe1—C24	2.054 (6)	C24—H24	0.9500
Fe1—C12	2.055 (6)	C25—H25	0.9500
Fe1—C14	2.064 (6)		
C13—Fe1—C23	109.3 (2)	C13—C12—H12	126.9
C13—Fe1—C15	68.3 (3)	C11—C12—H12	126.9
C23—Fe1—C15	155.3 (3)	Fe1—C12—H12	126.5
C13—Fe1—C22	124.8 (3)	C12—C13—C14	109.4 (6)
C23—Fe1—C22	40.7 (2)	C12—C13—Br13	125.0 (5)
C15—Fe1—C22	160.6 (3)	C14—C13—Br13	125.2 (5)
C13—Fe1—C11	68.1 (2)	C12—C13—Fe1	70.4 (3)
C23—Fe1—C11	163.6 (3)	C14—C13—Fe1	70.7 (4)
C15—Fe1—C11	40.3 (3)	Br13—C13—Fe1	130.6 (3)
C22—Fe1—C11	126.5 (3)	Br14—C14—C15	128.3 (8)
C13—Fe1—C21	160.7 (3)	Br14—C14—C13	124.9 (8)
C23—Fe1—C21	68.2 (2)	C15—C14—C13	106.8 (6)
C15—Fe1—C21	122.3 (3)	Br14—C14—Fe1	128.2 (9)
C22—Fe1—C21	40.8 (2)	C15—C14—Fe1	69.0 (4)
C11—Fe1—C21	108.6 (2)	C13—C14—Fe1	68.4 (4)
C13—Fe1—C25	158.4 (3)	C15—C14—H14	126.6

C23—Fe1—C25	68.1 (2)	C13—C14—H14	126.6
C15—Fe1—C25	104.6 (3)	Fe1—C14—H14	127.5
C22—Fe1—C25	68.2 (2)	C11—C15—C14	108.6 (6)
C11—Fe1—C25	120.6 (2)	C11—C15—Fe1	70.0 (4)
C21—Fe1—C25	40.2 (3)	C14—C15—Fe1	70.5 (4)
C13—Fe1—C24	122.9 (3)	C11—C15—H15	125.7
C23—Fe1—C24	40.4 (3)	C14—C15—H15	125.7
C15—Fe1—C24	118.6 (3)	Fe1—C15—H15	125.3
C22—Fe1—C24	68.6 (3)	C25—C21—C22	108.3 (5)
C11—Fe1—C24	155.0 (3)	C25—C21—Br21	125.3 (4)
C21—Fe1—C24	68.5 (3)	C22—C21—Br21	126.0 (5)
C25—Fe1—C24	41.0 (3)	C25—C21—Fe1	70.0 (4)
C13—Fe1—C12	40.8 (2)	C22—C21—Fe1	69.5 (3)
C23—Fe1—C12	126.6 (2)	Br21—C21—Fe1	131.4 (3)
C15—Fe1—C12	68.8 (3)	C25—C21—H21	125.8
C22—Fe1—C12	110.6 (3)	C22—C21—H21	125.8
C11—Fe1—C12	40.8 (2)	Fe1—C21—H21	126.2
C21—Fe1—C12	124.2 (3)	C23—C22—C21	107.3 (6)
C25—Fe1—C12	157.7 (3)	C23—C22—Br22	126.3 (4)
C24—Fe1—C12	161.0 (3)	C21—C22—Br22	126.1 (5)
C13—Fe1—C14	40.9 (3)	C23—C22—Fe1	69.3 (3)
C23—Fe1—C14	121.4 (3)	C21—C22—Fe1	69.7 (4)
C15—Fe1—C14	40.5 (3)	Br22—C22—Fe1	131.0 (3)
C22—Fe1—C14	158.8 (3)	C24—C23—C22	109.2 (5)
C11—Fe1—C14	68.0 (3)	C24—C23—Br23	125.2 (5)
C21—Fe1—C14	157.3 (3)	C22—C23—Br23	125.3 (5)
C25—Fe1—C14	120.7 (3)	C24—C23—Fe1	70.3 (3)
C24—Fe1—C14	104.6 (3)	C22—C23—Fe1	70.0 (3)
C12—Fe1—C14	68.9 (3)	Br23—C23—Fe1	130.2 (3)
C15—C11—C12	109.0 (6)	C23—C24—C25	106.8 (6)
C15—C11—Br11	125.9 (5)	C23—C24—Br24	131.1 (8)
C12—C11—Br11	124.9 (5)	C25—C24—Br24	121.9 (8)
C15—C11—Fe1	69.6 (3)	C23—C24—Fe1	69.2 (4)
C12—C11—Fe1	69.8 (3)	C25—C24—Fe1	69.4 (4)
Br11—C11—Fe1	130.3 (3)	Br24—C24—Fe1	123.0 (7)
C15—C11—H11	125.5	C23—C24—H24	126.6
C12—C11—H11	125.5	C25—C24—H24	126.6
Fe1—C11—H11	126.7	Fe1—C24—H24	126.3
C13—C12—C11	106.2 (6)	C21—C25—C24	108.4 (6)
C13—C12—Br12	126.8 (5)	C21—C25—Fe1	69.8 (4)
C11—C12—Br12	126.8 (5)	C24—C25—Fe1	69.6 (3)
C13—C12—Fe1	68.8 (3)	C21—C25—H25	125.8
C11—C12—Fe1	69.4 (3)	C24—C25—H25	125.8
Br12—C12—Fe1	130.2 (3)	Fe1—C25—H25	126.4

C15—C11—C12—C13	0.5 (6)	C25—C21—C22—C23	0.1 (6)
Br11—C11—C12—C13	−175.1 (4)	Br21—C21—C22—C23	173.6 (4)
Fe1—C11—C12—C13	59.2 (4)	Fe1—C21—C22—C23	−59.4 (4)

C15—C11—C12—Br12	175.8 (4)	C25—C21—C22—Br22	−173.9 (4)
Br11—C11—C12—Br12	0.3 (8)	Br21—C21—C22—Br22	−0.4 (8)
Fe1—C11—C12—Br12	−125.4 (5)	Fe1—C21—C22—Br22	126.6 (5)
C15—C11—C12—Fe1	−58.7 (4)	C25—C21—C22—Fe1	59.5 (4)
Br11—C11—C12—Fe1	125.7 (4)	Br21—C21—C22—Fe1	−127.0 (5)
C11—C12—C13—C14	0.7 (6)	C21—C22—C23—C24	0.1 (6)
Br12—C12—C13—C14	−174.7 (4)	Br22—C22—C23—C24	174.0 (4)
Fe1—C12—C13—C14	60.2 (4)	Fe1—C22—C23—C24	−59.6 (4)
C11—C12—C13—Br13	174.0 (4)	C21—C22—C23—Br23	−174.6 (4)
Br12—C12—C13—Br13	−1.4 (8)	Br22—C22—C23—Br23	−0.7 (7)
Fe1—C12—C13—Br13	−126.5 (4)	Fe1—C22—C23—Br23	125.7 (4)
C11—C12—C13—Fe1	−59.6 (4)	C21—C22—C23—Fe1	59.6 (4)
Br12—C12—C13—Fe1	125.1 (5)	Br22—C22—C23—Fe1	−126.4 (4)
C12—C13—C14—Br14	177.6 (11)	C22—C23—C24—C25	−0.1 (6)
Br13—C13—C14—Br14	4.3 (13)	Br23—C23—C24—C25	174.6 (4)
Fe1—C13—C14—Br14	−122.3 (11)	Fe1—C23—C24—C25	−59.5 (4)
C12—C13—C14—C15	−1.5 (7)	C22—C23—C24—Br24	175.6 (10)
Br13—C13—C14—C15	−174.8 (4)	Br23—C23—C24—Br24	−9.7 (12)
Fe1—C13—C14—C15	58.5 (4)	Fe1—C23—C24—Br24	116.2 (10)
C12—C13—C14—Fe1	−60.0 (4)	C22—C23—C24—Fe1	59.3 (4)
Br13—C13—C14—Fe1	126.7 (5)	Br23—C23—C24—Fe1	−126.0 (4)
C12—C11—C15—C14	−1.4 (7)	C22—C21—C25—C24	−0.1 (7)
Br11—C11—C15—C14	174.1 (4)	Br21—C21—C25—C24	−173.7 (4)
Fe1—C11—C15—C14	−60.2 (4)	Fe1—C21—C25—C24	59.0 (4)
C12—C11—C15—Fe1	58.8 (4)	C22—C21—C25—Fe1	−59.2 (4)
Br11—C11—C15—Fe1	−125.7 (4)	Br21—C21—C25—Fe1	127.3 (5)
Br14—C14—C15—C11	−177.3 (11)	C23—C24—C25—C21	0.2 (6)
C13—C14—C15—C11	1.8 (7)	Br24—C24—C25—C21	−176.0 (9)
Fe1—C14—C15—C11	59.9 (4)	Fe1—C24—C25—C21	−59.2 (4)
Br14—C14—C15—Fe1	122.8 (12)	C23—C24—C25—Fe1	59.4 (4)
C13—C14—C15—Fe1	−58.2 (4)	Br24—C24—C25—Fe1	−116.8 (9)

Bis(1,2,3,4-tetrabromocyclopentadienyl)iron(II) (compd_5)

Crystal data

$[Fe(C_5HBr_4)_2]$	$Z = 1$
$M_r = 817.25$	$F(000) = 368$
Triclinic, $P\overline{1}$	$D_x = 3.461$ Mg m^{-3}
$a = 6.9395$ (2) Å	Mo $K\alpha$ radiation, $\lambda = 0.71073$ Å
$b = 7.0548$ (2) Å	Cell parameters from 7252 reflections
$c = 8.9271$ (3) Å	$\theta = 3.0$–$36.2°$
$\alpha = 67.577$ (1)°	$\mu = 21.33$ mm^{-1}
$\beta = 76.160$ (1)°	$T = 103$ K
$\gamma = 86.461$ (1)°	Rod, yellow
$V = 392.06$ (2) Å^3	0.03 × 0.01 × 0.01 mm

Data collection

D8 Venture
diffractometer
Radiation source: rotating anode generator
Detector resolution: 7.4074 pixels mm^{-1}
mix of ω and phi scans
Absorption correction: multi-scan
(TWINABS; Bruker, 2012)
$T_{min} = 0.180$, $T_{max} = 0.344$

3772 measured reflections
3772 independent reflections
3107 reflections with $I > 2\sigma(I)$
$\theta_{max} = 36.3°$, $\theta_{min} = 3.0°$
$h = -11 \rightarrow 11$
$k = -10 \rightarrow 11$
$l = 0 \rightarrow 14$

Refinement

Refinement on F^2
Least-squares matrix: full
$R[F^2 > 2\sigma(F^2)] = 0.037$
$wR(F^2) = 0.076$
$S = 1.06$
3772 reflections
89 parameters
0 restraints
Primary atom site location: dual

Hydrogen site location: inferred from
neighbouring sites
H-atom parameters constrained
$w = 1/[\sigma^2(F_o^2) + (0.0237P)^2 + 1.5954P]$
where $P = (F_o^2 + 2F_c^2)/3$
$(\Delta/\sigma)_{max} = 0.001$
$\Delta\rho_{max} = 1.32$ e Å^{-3}
$\Delta\rho_{min} = -1.31$ e Å^{-3}

Special details

Geometry. All e.s.d.'s (except the e.s.d. in the dihedral angle between two l.s. planes) are estimated using the full covariance matrix. The cell e.s.d.'s are taken into account individually in the estimation of e.s.d.'s in distances, angles and torsion angles; correlations between e.s.d.'s in cell parameters are only used when they are defined by crystal symmetry. An approximate (isotropic) treatment of cell e.s.d.'s is used for estimating e.s.d.'s involving l.s. planes.

Refinement. Refined as a 2-component twin.

Fractional atomic coordinates and isotropic or equivalent isotropic displacement parameters (Å^2)

	x	y	z	U_{iso}*/U_{eq}
C1	0.2630 (5)	0.5035 (5)	0.3994 (4)	0.0110 (5)
C2	0.2568 (5)	0.6705 (5)	0.4545 (4)	0.0100 (5)
C3	0.2493 (5)	0.5846 (5)	0.6289 (4)	0.0095 (5)
C4	0.2505 (5)	0.3669 (5)	0.6804 (4)	0.0094 (5)
C5	0.2606 (5)	0.3150 (5)	0.5389 (4)	0.0094 (5)
H5	0.264990	0.180813	0.537579	0.011*
Br1	0.26938 (5)	0.52654 (6)	0.18277 (4)	0.01451 (7)
Br2	0.24350 (5)	0.94767 (5)	0.32428 (4)	0.01363 (7)
Br3	0.22892 (5)	0.73434 (5)	0.76565 (4)	0.01270 (7)
Br4	0.23435 (5)	0.17894 (5)	0.89794 (4)	0.01490 (7)
Fe1	0.500000	0.500000	0.500000	0.00706 (11)

Atomic displacement parameters (Å^2)

	U^{11}	U^{22}	U^{33}	U^{12}	U^{13}	U^{23}
C1	0.0120 (12)	0.0147 (14)	0.0079 (12)	0.0016 (10)	−0.0035 (10)	−0.0054 (11)
C2	0.0112 (11)	0.0101 (13)	0.0088 (12)	0.0018 (10)	−0.0030 (9)	−0.0036 (10)
C3	0.0109 (12)	0.0098 (13)	0.0070 (12)	−0.0002 (10)	−0.0006 (9)	−0.0033 (10)
C4	0.0099 (11)	0.0095 (13)	0.0076 (12)	−0.0002 (9)	−0.0010 (9)	−0.0024 (10)
C5	0.0112 (12)	0.0092 (13)	0.0076 (12)	0.0006 (10)	−0.0019 (10)	−0.0032 (10)

Br1	0.01640 (14)	0.01897 (17)	0.01080 (14)	0.00160 (12)	−0.00560 (11)	−0.00720 (12)
Br2	0.01950 (15)	0.00938 (14)	0.01115 (14)	0.00466 (11)	−0.00569 (11)	−0.00231 (11)
Br3	0.01718 (15)	0.01280 (15)	0.01024 (14)	0.00378 (11)	−0.00345 (11)	−0.00702 (11)
Br4	0.01921 (15)	0.01260 (15)	0.00856 (14)	−0.00057 (11)	−0.00061 (11)	−0.00070 (11)
Fe1	0.0084 (2)	0.0070 (3)	0.0056 (2)	0.00118 (19)	−0.0021 (2)	−0.0021 (2)

Geometric parameters (Å, º)

C1—C5	1.431 (5)	C3—Br3	1.874 (3)
C1—C2	1.434 (5)	C3—Fe1	2.036 (3)
C1—Br1	1.868 (3)	C4—C5	1.429 (5)
C1—Fe1	2.048 (3)	C4—Br4	1.869 (3)
C2—C3	1.427 (5)	C4—Fe1	2.046 (3)
C2—Br2	1.865 (3)	C5—Fe1	2.056 (3)
C2—Fe1	2.041 (3)	C5—H5	0.9500
C3—C4	1.426 (5)		
C5—C1—C2	108.6 (3)	C2^{i}—Fe1—C4	111.21 (13)
C5—C1—Br1	125.4 (3)	C2—Fe1—C4	68.79 (13)
C2—C1—Br1	125.9 (2)	C3^{i}—Fe1—C4^{i}	40.88 (13)
C5—C1—Fe1	69.90 (18)	C3—Fe1—C4^{i}	139.12 (13)
C2—C1—Fe1	69.19 (18)	C2^{i}—Fe1—C4^{i}	68.79 (13)
Br1—C1—Fe1	127.49 (17)	C2—Fe1—C4^{i}	111.21 (13)
C3—C2—C1	107.5 (3)	C4—Fe1—C4^{i}	180.0
C3—C2—Br2	126.5 (2)	C3^{i}—Fe1—C1^{i}	68.80 (13)
C1—C2—Br2	125.9 (2)	C3—Fe1—C1^{i}	111.20 (13)
C3—C2—Fe1	69.33 (18)	C2^{i}—Fe1—C1^{i}	41.06 (14)
C1—C2—Fe1	69.75 (18)	C2—Fe1—C1^{i}	138.94 (14)
Br2—C2—Fe1	129.31 (17)	C4—Fe1—C1^{i}	111.66 (13)
C4—C3—C2	108.0 (3)	C4^{i}—Fe1—C1^{i}	68.34 (13)
C4—C3—Br3	126.6 (2)	C3^{i}—Fe1—C1	111.20 (13)
C2—C3—Br3	125.3 (2)	C3—Fe1—C1	68.80 (13)
C4—C3—Fe1	69.94 (18)	C2^{i}—Fe1—C1	138.94 (14)
C2—C3—Fe1	69.68 (18)	C2—Fe1—C1	41.06 (14)
Br3—C3—Fe1	128.15 (17)	C4—Fe1—C1	68.34 (13)
C3—C4—C5	108.8 (3)	C4^{i}—Fe1—C1	111.66 (13)
C3—C4—Br4	125.8 (2)	C1^{i}—Fe1—C1	180.00 (8)
C5—C4—Br4	125.4 (2)	C3^{i}—Fe1—C5	110.92 (12)
C3—C4—Fe1	69.18 (17)	C3—Fe1—C5	69.08 (13)
C5—C4—Fe1	70.00 (17)	C2^{i}—Fe1—C5	110.77 (13)
Br4—C4—Fe1	128.05 (17)	C2—Fe1—C5	69.23 (13)
C4—C5—C1	107.1 (3)	C4—Fe1—C5	40.76 (13)
C4—C5—Fe1	69.24 (18)	C4^{i}—Fe1—C5	139.24 (13)
C1—C5—Fe1	69.29 (18)	C1^{i}—Fe1—C5	139.19 (13)
C4—C5—H5	126.5	C1—Fe1—C5	40.81 (13)
C1—C5—H5	126.5	C3^{i}—Fe1—C5^{i}	69.08 (13)
Fe1—C5—H5	126.6	C3—Fe1—C5^{i}	110.92 (13)
C3^{i}—Fe1—C3	180.0	C2^{i}—Fe1—C5^{i}	69.23 (13)

C3^i—Fe1—C2^i	40.99 (13)	C2—Fe1—C5^i	110.77 (13)
C3—Fe1—C2^i	139.01 (13)	C4—Fe1—C5^i	139.24 (13)
C3^i—Fe1—C2	139.01 (13)	C4^i—Fe1—C5^i	40.76 (13)
C3—Fe1—C2	40.99 (13)	C1^i—Fe1—C5^i	40.81 (13)
C2^i—Fe1—C2	180.0	C1—Fe1—C5^i	139.19 (13)
C3^i—Fe1—C4	139.12 (13)	C5—Fe1—C5^i	180.0
C3—Fe1—C4	40.88 (13)		

C5—C1—C2—C3	−0.4 (4)	Br3—C3—C4—C5	177.8 (2)
Br1—C1—C2—C3	178.8 (2)	Fe1—C3—C4—C5	−59.0 (2)
Fe1—C1—C2—C3	−59.3 (2)	C2—C3—C4—Br4	−177.9 (2)
C5—C1—C2—Br2	−176.6 (2)	Br3—C3—C4—Br4	−0.6 (4)
Br1—C1—C2—Br2	2.6 (4)	Fe1—C3—C4—Br4	122.6 (2)
Fe1—C1—C2—Br2	124.5 (3)	C2—C3—C4—Fe1	59.5 (2)
C5—C1—C2—Fe1	58.9 (2)	Br3—C3—C4—Fe1	−123.2 (3)
Br1—C1—C2—Fe1	−121.9 (3)	C3—C4—C5—C1	−0.8 (4)
C1—C2—C3—C4	−0.1 (4)	Br4—C4—C5—C1	177.7 (2)
Br2—C2—C3—C4	176.1 (2)	Fe1—C4—C5—C1	−59.2 (2)
Fe1—C2—C3—C4	−59.7 (2)	C3—C4—C5—Fe1	58.5 (2)
C1—C2—C3—Br3	−177.4 (2)	Br4—C4—C5—Fe1	−123.1 (2)
Br2—C2—C3—Br3	−1.3 (4)	C2—C1—C5—C4	0.7 (4)
Fe1—C2—C3—Br3	123.0 (2)	Br1—C1—C5—C4	−178.5 (2)
C1—C2—C3—Fe1	59.6 (2)	Fe1—C1—C5—C4	59.2 (2)
Br2—C2—C3—Fe1	−124.3 (3)	C2—C1—C5—Fe1	−58.5 (2)
C2—C3—C4—C5	0.5 (4)	Br1—C1—C5—Fe1	122.4 (3)

Symmetry code: (i) $-x+1, -y+1, -z+1$.

(1-Bromomercurio-2,3,4,5-tetrabromocyclopentadienyl)(1,2,3,4,5-pentabromocyclopentadienyl)iron(II) (compd_8)

Crystal data

[FeHgBr(C_5Br_4)(C_5Br_5)]
M_r = 1175.64
Monoclinic, $P2_1/n$
a = 8.9784 (3) Å
b = 14.0971 (4) Å
c = 15.8485 (4) Å
β = 90.689 (1)°
V = 2005.79 (10) Å^3
Z = 4
$F(000)$ = 2064
D_x = 3.893 Mg m^{-3}
Mo $K\alpha$ radiation, λ = 0.71073 Å
Cell parameters from 9571 reflections
θ = 2.6–26.1°
μ = 28.28 mm^{-1}
T = 295 K
Rod, yellow
0.06 × 0.02 × 0.02 mm

Data collection

D8 Venture diffractometer
Radiation source: rotating anode generator
Detector resolution: 7.4074 pixels mm^{-1}
mix of ω and phi scans
Absorption correction: multi-scan (SADABS; Krause *et al.*, 2015)
T_{min} = 0.193, T_{max} = 0.332
33353 measured reflections
4098 independent reflections
3154 reflections with $I > 2\sigma(I)$
R_{int} = 0.050
θ_{max} = 26.4°, θ_{min} = 2.9°
h = −11→11
k = −17→17
l = −19→19

Refinement

Refinement on F^2
Least-squares matrix: full
$R[F^2 > 2\sigma(F^2)] = 0.036$
$wR(F^2) = 0.092$
$S = 1.06$
4098 reflections
199 parameters
0 restraints
Primary atom site location: dual
$w = 1/[\sigma^2(F_o^2) + (0.0321P)^2 + 17.6846P]$
where $P = (F_o^2 + 2F_c^2)/3$
$(\Delta/\sigma)_{max} = 0.001$
$\Delta\rho_{max} = 1.63$ e Å^{-3}
$\Delta\rho_{min} = -1.24$ e Å^{-3}

Special details

Geometry. All e.s.d.'s (except the e.s.d. in the dihedral angle between two l.s. planes) are estimated using the full covariance matrix. The cell e.s.d.'s are taken into account individually in the estimation of e.s.d.'s in distances, angles and torsion angles; correlations between e.s.d.'s in cell parameters are only used when they are defined by crystal symmetry. An approximate (isotropic) treatment of cell e.s.d.'s is used for estimating e.s.d.'s involving l.s. planes.

Fractional atomic coordinates and isotropic or equivalent isotropic displacement parameters (Å^2)

	x	y	z	U_{iso}*/U_{eq}
C1	0.3728 (11)	0.6144 (7)	0.4691 (5)	0.048 (2)
C2	0.3219 (10)	0.5425 (6)	0.4119 (6)	0.046 (2)
C3	0.4378 (9)	0.5238 (6)	0.3545 (6)	0.0386 (19)
C4	0.5618 (9)	0.5838 (6)	0.3754 (5)	0.0376 (19)
C5	0.5205 (10)	0.6401 (6)	0.4451 (5)	0.041 (2)
C6	0.1984 (9)	0.7471 (6)	0.3246 (5)	0.0372 (19)
C7	0.2227 (9)	0.6896 (6)	0.2538 (5)	0.0381 (19)
C8	0.3692 (10)	0.7103 (6)	0.2257 (5)	0.0387 (19)
C9	0.4324 (9)	0.7793 (6)	0.2789 (5)	0.0360 (18)
C10	0.3276 (9)	0.8041 (6)	0.3418 (5)	0.0374 (19)
Br1	0.27025 (16)	0.66542 (10)	0.55928 (7)	0.0828 (4)
Br2	0.13919 (12)	0.48144 (10)	0.41585 (10)	0.0881 (5)
Br3	0.43841 (15)	0.43142 (8)	0.27139 (8)	0.0744 (4)
Br4	0.74361 (11)	0.58160 (8)	0.32153 (8)	0.0633 (3)
Br5	0.64199 (14)	0.73095 (8)	0.49869 (7)	0.0657 (3)
Br6	0.02030 (11)	0.75651 (8)	0.38521 (7)	0.0565 (3)
Br7	0.08463 (12)	0.61035 (8)	0.20025 (7)	0.0584 (3)
Br8	0.45641 (13)	0.65863 (9)	0.12890 (6)	0.0664 (3)
Br9	0.61817 (11)	0.83682 (8)	0.26468 (6)	0.0561 (3)
Br10	0.30895 (15)	1.00135 (9)	0.56050 (8)	0.0737 (3)
Fe1	0.37661 (12)	0.66252 (8)	0.34720 (7)	0.0310 (2)
Hg1	0.33752 (4)	0.89788 (3)	0.44073 (2)	0.04929 (13)

Atomic displacement parameters (Å^2)

	U^{11}	U^{22}	U^{33}	U^{12}	U^{13}	U^{23}
C1	0.055 (6)	0.053 (6)	0.035 (5)	0.012 (5)	0.013 (4)	0.018 (4)
C2	0.038 (5)	0.039 (5)	0.061 (6)	0.001 (4)	0.000 (4)	0.024 (4)
C3	0.038 (5)	0.029 (4)	0.049 (5)	0.000 (4)	−0.009 (4)	0.000 (4)
C4	0.036 (4)	0.035 (5)	0.042 (5)	0.001 (4)	0.003 (4)	0.002 (4)
C5	0.052 (5)	0.037 (5)	0.035 (4)	0.003 (4)	−0.007 (4)	0.001 (4)
C6	0.037 (4)	0.038 (5)	0.037 (4)	0.006 (4)	0.000 (4)	0.009 (4)

C7	0.042 (5)	0.039 (5)	0.033 (4)	0.002 (4)	−0.004 (4)	0.006 (4)
C8	0.046 (5)	0.040 (5)	0.030 (4)	0.002 (4)	0.003 (4)	0.002 (4)
C9	0.039 (5)	0.035 (5)	0.033 (4)	−0.002 (4)	0.001 (3)	0.011 (4)
C10	0.042 (5)	0.028 (4)	0.042 (5)	−0.001 (4)	−0.003 (4)	0.006 (4)
Br1	0.0975 (9)	0.1086 (10)	0.0430 (6)	0.0443 (8)	0.0300 (6)	0.0162 (6)
Br2	0.0453 (6)	0.0826 (9)	0.1366 (12)	−0.0178 (6)	0.0029 (7)	0.0531 (9)
Br3	0.0965 (9)	0.0442 (6)	0.0819 (8)	0.0015 (6)	−0.0275 (7)	−0.0233 (6)
Br4	0.0380 (5)	0.0672 (7)	0.0849 (8)	0.0044 (5)	0.0131 (5)	−0.0040 (6)
Br5	0.0853 (8)	0.0504 (6)	0.0606 (6)	0.0006 (5)	−0.0303 (6)	−0.0166 (5)
Br6	0.0387 (5)	0.0638 (6)	0.0673 (6)	0.0041 (4)	0.0110 (5)	0.0041 (5)
Br7	0.0510 (6)	0.0672 (7)	0.0566 (6)	−0.0122 (5)	−0.0081 (5)	−0.0058 (5)
Br8	0.0728 (7)	0.0840 (8)	0.0426 (5)	−0.0054 (6)	0.0139 (5)	−0.0096 (5)
Br9	0.0541 (6)	0.0614 (6)	0.0532 (6)	−0.0209 (5)	0.0129 (5)	0.0008 (5)
Br10	0.0875 (9)	0.0667 (7)	0.0670 (7)	−0.0043 (6)	0.0120 (6)	−0.0210 (6)
Fe1	0.0313 (6)	0.0302 (6)	0.0316 (6)	0.0001 (5)	0.0034 (4)	0.0027 (5)
Hg1	0.0585 (2)	0.0407 (2)	0.0488 (2)	−0.00033 (17)	0.00521 (17)	−0.00432 (17)

Geometric parameters (Å, º)

C1—C5	1.431 (13)	C6—C10	1.434 (12)
C1—C2	1.432 (14)	C6—Br6	1.880 (8)
C1—Br1	1.855 (9)	C6—Fe1	2.024 (8)
C1—Fe1	2.049 (8)	C7—C8	1.424 (12)
C2—C3	1.415 (13)	C7—Br7	1.866 (9)
C2—Br2	1.855 (9)	C7—Fe1	2.048 (8)
C2—Fe1	2.041 (8)	C8—C9	1.404 (12)
C3—C4	1.434 (11)	C8—Br8	1.877 (8)
C3—Br3	1.852 (9)	C8—Fe1	2.041 (8)
C3—Fe1	2.034 (8)	C9—C10	1.422 (11)
C4—C5	1.413 (12)	C9—Br9	1.870 (8)
C4—Br4	1.852 (8)	C9—Fe1	2.037 (8)
C4—Fe1	2.044 (8)	C10—Fe1	2.045 (8)
C5—Br5	1.879 (9)	C10—Hg1	2.052 (9)
C5—Fe1	2.032 (8)	Br10—Hg1	2.4101 (12)
C6—C7	1.403 (12)		
C5—C1—C2	107.5 (8)	Br9—C9—Fe1	129.8 (4)
C5—C1—Br1	125.3 (8)	C9—C10—C6	105.6 (7)
C2—C1—Br1	127.3 (7)	C9—C10—Fe1	69.3 (5)
C5—C1—Fe1	68.9 (5)	C6—C10—Fe1	68.6 (5)
C2—C1—Fe1	69.2 (5)	C9—C10—Hg1	132.1 (6)
Br1—C1—Fe1	127.8 (5)	C6—C10—Hg1	122.3 (6)
C3—C2—C1	107.9 (8)	Fe1—C10—Hg1	126.1 (4)
C3—C2—Br2	126.4 (7)	C6—Fe1—C5	136.1 (3)
C1—C2—Br2	125.6 (7)	C6—Fe1—C3	142.1 (3)
C3—C2—Fe1	69.4 (5)	C5—Fe1—C3	68.8 (3)
C1—C2—Fe1	69.8 (5)	C6—Fe1—C9	68.2 (3)
Br2—C2—Fe1	128.3 (5)	C5—Fe1—C9	111.9 (4)

C2—C3—C4	108.4 (8)	C3—Fe1—C9	137.7 (4)
C2—C3—Br3	126.6 (7)	C6—Fe1—C8	67.8 (3)
C4—C3—Br3	124.8 (6)	C5—Fe1—C8	141.7 (4)
C2—C3—Fe1	69.9 (5)	C3—Fe1—C8	112.1 (3)
C4—C3—Fe1	69.8 (5)	C9—Fe1—C8	40.3 (3)
Br3—C3—Fe1	129.7 (5)	C6—Fe1—C2	112.5 (3)
C5—C4—C3	107.6 (7)	C5—Fe1—C2	69.0 (4)
C5—C4—Br4	127.6 (7)	C3—Fe1—C2	40.6 (4)
C3—C4—Br4	124.7 (6)	C9—Fe1—C2	177.9 (4)
C5—C4—Fe1	69.3 (5)	C8—Fe1—C2	137.9 (4)
C3—C4—Fe1	69.1 (5)	C6—Fe1—C4	176.2 (4)
Br4—C4—Fe1	128.9 (4)	C5—Fe1—C4	40.6 (3)
C4—C5—C1	108.6 (8)	C3—Fe1—C4	41.2 (3)
C4—C5—Br5	125.5 (7)	C9—Fe1—C4	110.5 (3)
C1—C5—Br5	126.0 (7)	C8—Fe1—C4	113.7 (3)
C4—C5—Fe1	70.2 (5)	C2—Fe1—C4	68.9 (3)
C1—C5—Fe1	70.1 (5)	C6—Fe1—C10	41.3 (3)
Br5—C5—Fe1	126.8 (5)	C5—Fe1—C10	108.6 (3)
C7—C6—C10	110.0 (7)	C3—Fe1—C10	176.6 (3)
C7—C6—Br6	126.2 (7)	C9—Fe1—C10	40.8 (3)
C10—C6—Br6	123.7 (6)	C8—Fe1—C10	68.5 (3)
C7—C6—Fe1	70.8 (5)	C2—Fe1—C10	141.0 (4)
C10—C6—Fe1	70.2 (5)	C4—Fe1—C10	135.5 (3)
Br6—C6—Fe1	128.8 (4)	C6—Fe1—C7	40.3 (3)
C6—C7—C8	106.6 (7)	C5—Fe1—C7	176.3 (4)
C6—C7—Br7	126.9 (6)	C3—Fe1—C7	113.6 (3)
C8—C7—Br7	126.2 (6)	C9—Fe1—C7	68.5 (3)
C6—C7—Fe1	68.9 (5)	C8—Fe1—C7	40.8 (3)
C8—C7—Fe1	69.3 (5)	C2—Fe1—C7	110.7 (4)
Br7—C7—Fe1	131.0 (5)	C4—Fe1—C7	143.0 (3)
C9—C8—C7	108.8 (7)	C10—Fe1—C7	69.2 (3)
C9—C8—Br8	126.2 (6)	C6—Fe1—C1	109.9 (3)
C7—C8—Br8	124.9 (6)	C5—Fe1—C1	41.0 (4)
C9—C8—Fe1	69.7 (5)	C3—Fe1—C1	68.6 (4)
C7—C8—Fe1	69.9 (5)	C9—Fe1—C1	140.9 (4)
Br8—C8—Fe1	129.4 (5)	C8—Fe1—C1	177.2 (4)
C8—C9—C10	109.0 (7)	C2—Fe1—C1	41.0 (4)
C8—C9—Br9	125.6 (6)	C4—Fe1—C1	68.7 (3)
C10—C9—Br9	125.2 (6)	C10—Fe1—C1	110.9 (4)
C8—C9—Fe1	70.0 (5)	C7—Fe1—C1	136.4 (4)
C10—C9—Fe1	69.9 (5)	C10—Hg1—Br10	171.0 (2)